Agricultural and Forest Meteorology 291 (2020) 108088

Contents lists available at ScienceDirect

Agricultural and Forest Meteorology

journal homepage: www.elsevier.com/locate/agrformet

Review

Value of sun-induced chlorophyll fluorescence for quantifying hydrological states and fluxes: Current status and challenges

F. Jonard[a,b,*], S. De Cannière[b], N. Brüggemann[a], P. Gentine[c], D.J. Short Gianotti[d], G. Lobet[a,b], D.G. Miralles[e], C. Montzka[a], B.R. Pagán[e], U. Rascher[f], H. Vereecken[a]

[a] Agrosphere (IBG-3), Institute of Bio- and Geosciences, Forschungszentrum Jülich GmbH, Germany
[b] Earth and Life Institute, Université catholique de Louvain, Belgium
[c] Department of Earth and Environmental Engineering, Columbia University, New York, NY, United States
[d] Parsons Laboratory, Department of Civil and Environmental Engineering, Massachusetts Institute of Technology, Cambridge, MA, United States
[e] Hydro-Climate Extremes Lab (H-CEL), Ghent University, Belgium
[f] Plant Sciences (IBG-2), Institute of Bio- and Geosciences, Forschungszentrum Jülich GmbH, Germany

ARTICLE INFO

Keywords:
Solar-induced chlorophyll fluorescence
Soil water availability
Drought stress
Transpiration
Hydrological processes
Radiative transfer model

ABSTRACT

Predictions of hydrological states and fluxes, especially transpiration, are poorly constrained in hydrological models due to large uncertainties in parameterization and process description. Novel technologies like remote sensing of sun-induced chlorophyll fluorescence (SIF)—which provides information from the photosynthetic apparatus—may help in constraining water cycle components. This paper discusses the nature of the plant physiological basis of the fluorescence signal and analyses the current literature linking hydrological states and fluxes to SIF. Given the connection between photosynthesis and transpiration, through the water use efficiency, SIF may serve as a pertinent constraint for hydrological models. The FLuorescence EXplorer (FLEX) satellite, planned to be launched in 2023, is expected to provide spatially high-resolution measurements of red and far-red SIF complementing the products from existing satellite missions and the high-temporal resolution products from upcoming geostationary missions. This new data stream may allow us to better constrain plant transpiration, assess the impacts of water stress on plants, and infer processes occurring in the root zone through the soil-plant water column. To make optimal use of this data, progress needs to be made in 1) our process representation of spatially aggregated fluorescence signals from spaceborne SIF instruments, 2) integration of fluorescence processes in hydrological models—particularly when paired with other satellite data, 3) quantifying the impact of soil moisture on SIF across scales, and 4) assessment of the accuracy of SIF measurements—especially from space.

1. Introduction

Photosynthesis is the process of converting light energy into chemical energy stored as carbohydrates. These carbohydrates are synthesized from atmospheric carbon dioxide and water taken up by the roots and delivered by the xylem to the different plant organs. Photosynthesis is controlled by two photosystems: photosystem I (PSI) and photosystem II (PSII), located in the leaves. These photosystems are pigment-containing protein complexes that contain reaction centres where photochemical reactions occur (Reed, 1969). Following the absorption of incoming photosynthetically active radiation (PAR) by chlorophyll ($APAR_{Chl}$) (Zhang et al., 2018c), most of the incoming radiation is converted into energy for photosynthesis (often referred to as photochemical quenching, PQ), yet some of the energy is dissipated as heat for photoprotection (often referred to as non-photochemical quenching, NPQ), and a small fraction is re-emitted back as chlorophyll fluorescence (ChlF) at wavelengths between 650 and 800 nm (Kautsky and Hirsch, 1931). Subsequently, the fluorescence signal originating from the photosystems is a potential indicator of plant photosynthetic activity.

Photosynthesis strongly depends on environmental variables, such as soil and leaf water potentials, water vapour pressure deficit, or soil nutrient concentration (Jarvis, 1976). The measurement of ChlF might therefore provide valuable information on how these environmental variables control photosynthesis. While ChlF has been investigated for nearly a century, mainly under laboratory conditions and by using active detection methods, many questions remain. How does ChlF emission change in function of photosynthetic activity? What is the impact

* Corresponding author.
E-mail address: f.jonard@fz-juelich.de (F. Jonard).

https://doi.org/10.1016/j.agrformet.2020.108088
Received 13 October 2019; Received in revised form 12 June 2020; Accepted 15 June 2020
Available online 22 June 2020

of drought stress on ChlF emission? Better understanding the behaviour of the ChlF emission at different scales (from chloroplast to ecosystem)—and how this emission is driven by stress-induced changes in photosystem-level ChlF emission and in canopy structure (Dechant et al., 2020)—may provide opportunities to improve estimation of photosynthesis using water cycle state variables and to use subtle changes in photosynthesis to better predict transpiration (Frankenberg and Berry, 2018; Gentine and Alemohammad, 2018; Gu et al., 2019; Zhang et al., 2018a).

Fluorescence measurements can be performed at different spatial scales (from the leaf to the ecosystem scale) and temporal resolutions (from seconds to years). The different measurement techniques can be classified as active and passive. Active systems use an artificial source of energy to excite ChlF, while passive systems measure ChlF induced by the absorption of sunlight. Active methods use light pulses of different intensities. The shape of the fluorescence response to these pulses, as well as the relative height of the different pulse-induced peaks, provide information about the state of photosynthesis (Govindje, 1995), therefore enabling the detection of abiotic stresses, including drought (Stirbet et al., 2018). The current standard in active fluorescence is the Pulse-Amplitude Modulation (PAM) (Schreiber et al., 1986). The more recent laser-induced fluorescence transient (LIFT) sensor sends a saturation pulse using laser as illumination source (Keller et al., 2019a, 2019b). This allows measuring active fluorescence at the canopy scale.

Passive techniques can measure sun-induced chlorophyll fluorescence (SIF) over large scales thanks to advances in spectrometer technology in terms of spectral resolution and accuracy during the last decade (Meroni et al., 2009; Mohammed et al., 2019). Unlike active measurements, they rely on the absolute value of the emitted fluorescence under natural light conditions, and therefore are dependant on the absorbed radiation and the information content of SIF is lower than one can expect from active approaches. As SIF amounts to only ~1–3% of the absorbed shortwave radiation, it can only be measured in specific spectral bands, in which solar irradiation is reduced (Krause and Weis, 1991). An important method for measuring SIF is the Fraunhofer line discriminator/depth (FLD) method, based on the radiations measured in these specific bands (Carter et al., 1996; Moya et al., 2004; Plascyk, 1975; Theisen, 2002). Passive systems are generally applied at canopy to ecosystem level. Global retrievals of SIF have been achieved from spaceborne spectrometers. These sensors were not initially designed for measuring SIF but rather to monitor atmospheric trace gases. These sensors include the ENVIronmental SATellite (EnviSat) – SCanning Imaging Absorption spectroMeter for Atmospheric CHartographY (SCIAMACHY), the Greenhouse gases Observing SATellite (GOSAT) – Thermal And Near-infrared Sensor for carbon Observation-Fourier Transform Spectrometer (TANSO-FTS), the Meteorological Operational (MetOp) satellites – Global Ozone Monitoring Experiment-2 (GOME-2) instruments, the Orbiting Carbon Observatory (OCO-2), the Sentinel-5 Precursor (S-5P) – TROPOspheric Monitoring Instrument (TROPOMI) and the Carbon Dioxide Observation Satellite (TanSat) – Atmospheric Carbon dioxide Grating Spectrometer (ACGS) (Du et al., 2018; Frankenberg et al., 2011, 2014; Guanter et al., 2012; Joiner et al., 2011; Köhler et al., 2018, 2015; Sun et al., 2018). Due to the large interest of the scientific community in SIF, the European Space Agency has planned to launch the FLuorescence EXplorer (FLEX) satellite in 2023. FLEX will carry the first very high-resolution spectrometer dedicated specifically to globally map fluorescence providing instantaneous measurements of both fluorescence peaks (red and far-red fluorescence peaks) along with reflectance in the visible and near-infrared spectral window (Drusch et al., 2017).

Early studies of ChlF have mainly focused on the relation between ChlF and photosynthetic activity or carbon assimilation at the leaf level (Govindje, 1995). More recently, with increased developments in passive measurement techniques allowing estimates of SIF over large spatial scales, several research initiatives have investigated the value of SIF as a constraint for land surface models, in particular for gross primary production (GPP) of vegetation canopies (Frankenberg et al., 2011; Guanter et al., 2014; MacBean et al., 2018; Wieneke et al., 2016) and crop yield (Guan et al., 2016). As photosynthesis is closely linked to hydrological processes, information on SIF may help to illuminate processes within the soil-plant-atmosphere continuum, particularly to constrain transpiration fluxes (Ač et al., 2015; Alemohammad et al., 2017; Cendrero-Mateo et al., 2015; Lu et al., 2018; Pagan et al., 2019; Shan et al., 2019) as well as to better quantify light and water use efficiencies (LUE and WUE) of plants (Short Gianotti et al., 2019).

Here, we review current knowledge on the potential of SIF to provide information on hydrological processes with a focus on the use of SIF to better constrain plant transpiration, potentially allowing for early plant water stress detection, i.e., prior to the appearance of visible range symptoms (e.g., browning), and how it can potentially be used to infer processes in the root zone. Monitoring plant water stress and root-zone soil moisture is of major interest, in particular, to optimize irrigation in water-limited areas and to mitigate the impacts of drought events, which are expected to increase in frequency and intensity in the wake of global warming (IPCC, 2014). This review is organized in four sections. Section 2 analyses the physiological responses of plants to soil moisture and drought and provides an overview of the findings from experimental physiology studies on the relationship between plant water status and chlorophyll fluorescence. In Section 3, we evaluate the potential of remotely-sensed SIF measurements to improve hydrological state and flux estimates. Finally, in Section 4, we provide a conclusion and discuss further research avenues to explore.

2. Physiological response of plants to drought

2.1. Photosynthetic response of plants to drought

Photosynthetic response to low soil water potential is complex. Between the dry soil with low water potential and the site of photosynthesis, the path of water is regulated at many sites in the plant (Fig. 1).

Locally, the hydraulic conductivity of soil and roots varies with soil water potential, especially in the vicinity of fine roots (Siqueira et al., 2009). On short time scales (minutes to hours), water channels, or aquaporins, can be downregulated or gated as soil water potential

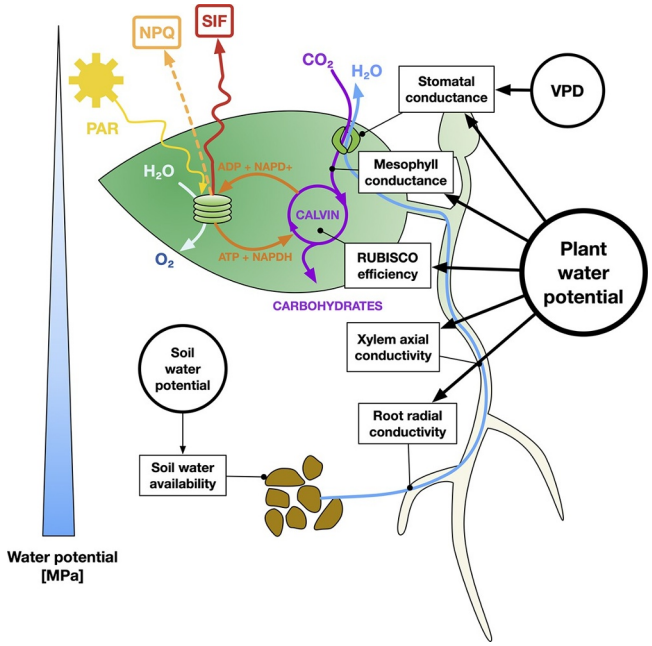

Fig. 1. Overview of plant scale processes and water potential gradient in the soil–plant–atmosphere continuum.

decreases and thus reduce the flow of water between cells (Cochard et al., 2007b; Hachez et al., 2012). On longer time scales (hours to days), root segments growing in soil regions with low soil water potential can also develop hydrophobic barriers by depositing suberin, a hydrophobic compound, in specific root layers (Barberon et al., 2016; Doblas et al., 2017; Enstone and Peterson, 2005). These two processes have the direct effect of hydraulically isolating the root from its direct dry environment, hence preventing a drop in internal xylem water potential. The sensitivity of such response has been shown to be variable between plant species (Hose et al., 2000; Martinez-Ballesta et al., 2003).

A second layer of control lies within the network of xylem vessels. Xylem vessels are designed to conduct water efficiently within the plant from the roots to the leaves. However, when the water tension within the vessels becomes too high, embolism (cavitation) events can occur, i.e., gas bubbles start to form. Wherever cavitation occurs, the hydraulic conductivity of the corresponding xylem element drops, blocking the flow in that part of the xylem. Cavitation of xylem vessels is usually not permanent, and plants can often refill the embolized vessels (Zwieniecki and Holbrook, 2009), however, this refiling process can vary from plant to plant (Cochard et al., 2008, 2007a; Rewald et al., 2011). Reduction in the conductivity of the xylem and the drop in soil water potential in combination with the effect of vapour pressure deficit (VPD, high VPD leading to stomatal closure) (Jarvis, 1976; Zhou et al., 2019) together reduce the leaf water potential, influencing photosynthesis and stomatal aperture (Jonard et al., 2011; Kennedy et al., 2019).

A first photosynthesis impairment under drought conditions is by stomatal limitation. Due to the decrease in water potential within the substomatal cavities and hormonal triggers, stomata may partially close, reducing the amount of CO_2 entering the plant and therefore decreasing photosynthesis, and at the same time reducing the flux of vapour into the atmosphere through transpiration (Lemordant and Gentine, 2019; Lemordant et al., 2016). The sensitivity of guard cells to hydraulic and hormonal signals (Acharya and Assmann, 2009; Christmann et al., 2007; Tardieu et al., 2015) determines the plant water response. Plants with a near-isohydric behaviour limit xylem cavitation through early stomatal closure, while plants with more anisohydric behaviour keep their stomata more open while drought progresses, thus sustaining higher transpiration rates (Cochard, 2002; Huber et al., 2014; Konings and Gentine, 2017; Martin-StPaul et al., 2017; Novick et al., 2019; Sperry et al., 2016). These two strategies can be species-specific (e.g., sunflower is isohydric, while maize is anisohydric), but also genotype-specific, as observed in tomatoes (Sade et al., 2012, 2009) or even vary with drought level.

The second form of response occurring under drought conditions is a non-stomatal limitation of photosynthesis. This limitation is measured as the change in the ratio between the net CO_2 assimilation rate and the leaf-internal CO_2 concentration (*A-Ci* curve) (Long and Bernacchi, 2003; Zhou et al., 2013), which can be divided into two components. The first is the reduction of the mesophyll conductance to CO_2 (Flexas et al., 2016). This limitation can be large and is thought to be due to a down-regulation of aquaporins (Flexas et al., 2006). The second type of non-stomatal limitation is linked to a reduction in the metabolic efficiency of the enzyme Rubisco due to a reduction in CO_2 availability (Grassi and Magnani, 2005). Under normal conditions, there is a strong coordination between Rubisco and the CO_2 diffusional characteristics of leaves. However, under prolonged water deficit (several days), this coordination is lost and diffusional limitations to photosynthesis become dominant (Galmes et al., 2017). Under prolonged water deficit, more structural damages can also appear in the photosynthesis apparatus, such as the deterioration of thylakoid membranes (Sperdouli and Moustakas, 2012).

The relative contribution of the stomatal and non-stomatal limitations is not constant and varies between species (Galmes et al., 2007; Zhou et al., 2015), cultivars (Bota et al., 2016), developmental stages (Egea et al., 2011; Grassi and Magnani, 2005) and stress severity (Galmes et al., 2007). Over longer periods of severe water stress, leaf area per plant decreases, as does chlorophyll density within leaves, xylem conductivity, and vegetated-to-bare soil ratio.

2.2. Fluorescence response of plants to drought

Stomatal and non-stomatal responses to drought result in a lower internal CO_2 in the sub-stomatal chambers, reducing the efficiency of the Calvin cycle. This leads to a lower demand of ATP and NADPH which, in turn, slows down the photosynthetic electron transport (Vanlerberghe et al., 2016). The lowered ATPase activity causes protons to accumulate in the thylakoids, resulting in a pH gradient over the thylakoid membrane (Campos et al., 2014; Cousins et al., 2002). The increased pH gradient over the thylakoid membrane triggers an increase in non-photochemical quenching (NPQ). NPQ covers a variety of biochemical and biophysical processes that dissipate the excessive energy from the photosystems, avoiding the formation of radical species and the concomitant destruction of the photosynthetic complexes (see Jahns and Holzwarth, 2012; Niyogi and Truong, 2013; Ruban, 2016 for an overview on this topic). The increased pH gradient also causes kinases to move light-harvesting complex II (LHCII) from PSII to PSI (Campos et al., 2014; Kruger et al., 2012; Rochaix, 2007). The PSI-bound LHCII provides photoprotection for PSI. Unlike for linear electron transport, cyclic electron transport does not produce NADPH, allowing adaptation to the decreased Calvin cycle activity (Fig. 2) (Rochaix, 2007; Zivcak et al., 2013).

A second process modulating the transfer of energy to the photosynthetic electron transport chain is the ‘damage and repair cycle’ of PSII (Jin et al., 2003). An overstimulation of PSII leads to the production of singlet oxygen, inducing reversible damage to the PSII. If the damage occurs at a faster rate than the repair, the downstream energy transfer is slowed down. This phenomenon is called photoinhibition (Demmig-Adams et al., 2012; Murata et al., 2012). The movement of the light-harvesting complexes and the increased pH gradient over the thylakoid membrane alters the partitioning of energy between the pathways of photosynthesis, heat dissipation and fluorescence, the latter two providing an alternative electron sink to photosynthesis. The effect of drought stress on the fluorescence itself differs at the photosystem level. Upon overstimulation, either by over-illumination or by a reduced plastoquinone pool, the sum of the energy dissipated by both PSII ChlF and NPQ increases, protecting PSII from photobleaching. In an overstimulated PSI, the PSI primary electron donor (P700) itself acts as a quencher, i.e., it will dissipate the excess incoming energy (Porcar-Castell et al., 2014).

In addition, other environmental factors can interact with drought stress and influence the photosynthetic efficiency and fluorescence emission. Nitrogen (N), for instance, is an important component in the synthesis of photosynthetic pigments and Rubisco. As such, N availability can play a role in the response of photosynthesis to drought stress. In winter wheat, an appropriate level of N supply has been shown to improve the photosynthesis response to decreasing soil water content and to decrease the effect of drought stress (Wang et al., 2016). Low N levels, in combination with drought, can lead to more severe reductions of photosynthesis (Wang et al., 2016; Wu et al., 2008).

There are only very limited studies available on the link between low temperatures (chilling) and SIF. Ač et al. (2015) found in their meta-analysis a larger increase in far-red fluorescence compared to red fluorescence in response to chilling stress, which could be attributed to a reduction of PQ. Other studies using active fluorescence methods seem to support this and, for example, Lin et al. (2007) observed an increase in minimal fluorescence yield in dark-adapted state (F_0) because of chilling stress. Wang et al. (2016) observed a decrease in thylakoid membrane fluidity, blocking electron transfer in the PSII reaction centres and reducing NPQ, also resulting in an increased fluorescence. High temperature (heat) stress is often associated with drought

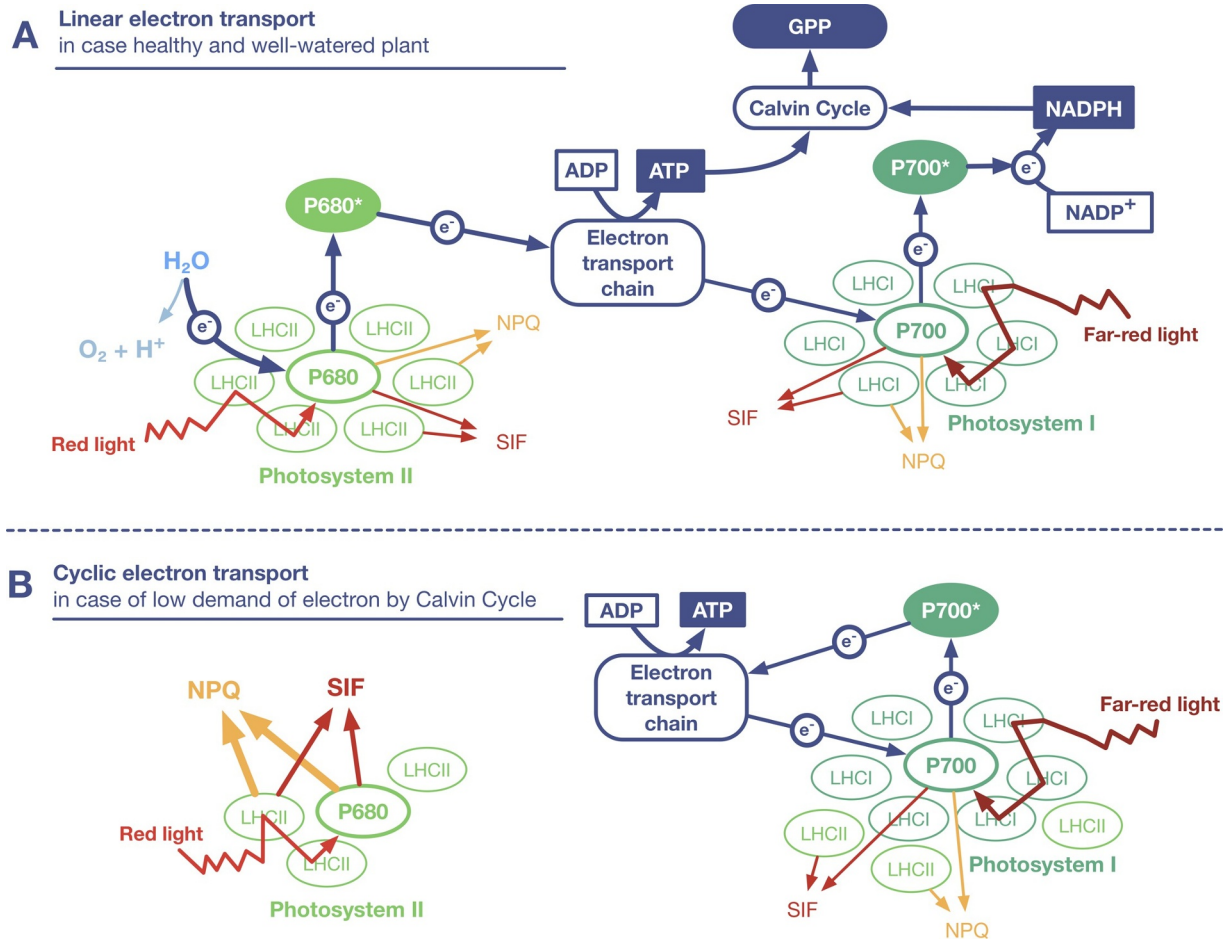

Fig. 2. Visualization of linear (A) and cyclic (B) electron transport in photosynthesis.

stress, as high air temperatures increase the atmospheric vapour pressure deficit (see also Section 3.5.). In addition to the drought effect, heat stress tends to damage the chloroplast membranes, changing the activity of various proteins (Feng et al., 2014). Consequently heat stress results in a decrease in both red and far-red fluorescence (Ač et al., 2015).

2.3. Link between soil moisture and fluorescence: findings from experimental studies

Various experimental studies have explored the potential of specific parameters derived from active measurements of chlorophyll fluorescence to provide information on soil moisture status in the root zone. Analysis of existing literature shows contradictory information about the effect of soil moisture on ChlF. Depending on the studied species, and the type and intensity of the stress applied, either no effect, a positive, or a negative effect of soil moisture were observed on parameters related to active measurements of ChlF (Table 1). These diverse results may be partly explained by the non-uniformity in the studied stress duration, the type of plant, type of soil or also the soil moisture levels imposed in these studies. As the relationship is nonlinear in nature and depends on the range of soil moisture values, range of dependence may be found, while for high soil moisture values, minimal stress is expected. While some studies report soil moisture only in qualitative wet/dry terms (e.g., Pettigrew (2004)), even quantitative inter-comparison of the soil moisture/ChlF relationship across studies is hampered by difficulty converting between gravimetric (Kebbas et al., 2015; Man et al., 2017; Xia et al., 2014; Xu and Zhou, 2011), volumetric (Gajanayake and Reddy, 2016; Lang et al., 2018; Ohashi et al., 2006; Trigo-Cordoba et al., 2015), and soil water potential (Li et al., 2004; Snider et al., 2014; Vincent et al., 2015) methods without sufficient reported soil characteristics for inter-conversion. To some degree, this is a disciplinary disconnect between hydrological and physiological lenses. Necessary root zone variables to fully determine the soil moisture/ChlF relationship are soil water potential—preferably as a profile in depth, root water potential, and magnitude and duration of soil moisture deficits.

3. Lessons from remote sensing data

3.1. Remote sensing of SIF

In remote sensing, vegetation monitoring is traditionally based on reflectance-based spectral vegetation indices (VIs) diagnosing leaf chlorophyll content, biomass, canopy structure, and fractional cover (Gentine and Alemohammad, 2018; Mulla, 2013; Stocker et al., 2019). However, these indices only indirectly relate to actual vegetation activity so that additional data and modelling steps are required (Guanter et al., 2014). Canopy structure and its dynamics can also be assessed by passive microwave remote sensing of vegetation optical depth (VOD), which is related to dry biomass and relative water content (Konings et al., 2017; Momen et al., 2017; Vereecken et al., 2012; Zhang et al., 2019). As a by-product of photosynthesis, SIF can be indicative of the rate of actual photosynthesis within the plant. Active pulse-modulation or illumination with a saturating light pulse cannot currently be performed at ecosystem scale. Therefore, passive methods have been prioritised in remote sensing of fluorescence (Malenovský et al., 2009; Meroni et al., 2009; Mohammed et al., 2019; Porcar-

Table 1
Overview of a selection of studies linking fluorescence parameters (using active fluorescence methods) and drought stresses. For each study, the effect of the stress on fluorescence parameters, i.e., null (0), negative (-) or positive (+), the type of stress, and the type of soil moisture measurement were compiled (Φ_{PSII}: quantum yield of photosystem II electron transport; ETR: electron transport rate; F_v/F_m: maximal efficiency of PSII after dark adaption; F_s: steady-state fluorescence yield in light-adapted state; F_0: minimal fluorescence yield after dark adaption; NPQ: non-photochemical quenching; g_s: stomatal conductance).

Plant species	Effect of stress on ChlF						Stress type	Soil moisture measurement	Reference
	Φ_{PSII}	ETR	F_v/F_m	F_s	F_0	NPQ			
Gossypium hirsutum	0	0					drought	soil water potential	Snider et al. (2014)
Acacia tortilis	–	–				+	drought	gravimetric	Kebbas et al. (2015)
Glycine max		–	–				drought	volumetric	Ohashi et al. (2006)
Vitis vinifera	0	0	0	+		+	drought	volumetric	Trigo-Cordoba et al. (2015)
Solanum tuberosum	0				–	+	drought	soil moisture deficit	Jefferies (1992)
Medicago sativa			–				salinity	none	Latrach et al. (2014)
Cucumis sativus	–		–		–	+	salinity	none	Stepien and Klobus (2006)
Triticum aestivum	–		–				drought	gravimetric	Man et al. (2017)
Ziziphus jujuba	–		–			+	drought	gravimetric	Xia et al. (2014)
Stipa grandis	–	–	–				drought	gravimetric	Xu and Zhou (2011)
Leymus chinensis	–	–	–				drought	gravimetric	Xu and Zhou (2011)
Forsythia suspensa	–		–		+	+	drought	volumetric	Lang et al. (2018)
Ipomoea batatas	–						drought	volumetric	Gajanayake and Reddy (2016)
Phaseolus vulgaris	0					+	g_s reduction	none	Omasa and Takayama (2003)
Carica papaya			0				drought	soil water potential	Vincent et al. (2015)
Vitis vinifera		–				+	drought	none	Flexas et al. (2002a)
Vitis vinifera		0				+	drought	none	Flexas et al. (2002b)
Vitis vinifera		–	–	–			drought	none	Flexas et al. (2000)
Vitis vinifera		–					drought	none	Medrano et al. (2002)
Oryza sativa		–	–		+	+	drought	irrigation deficit	Xu et al. (2020)
Zea mays			–	+		+	drought	none	Chen et al. (2018)
Arabidopsis thaliana	–			+		+	drought	none	Mishra et al. (2016)
Gossypium hirsutum	–	–	0			+	drought	none	Pettigrew (2004)
Typha latifolia		–	0		+	0	drought	soil water potential	Li et al. (2004)

Castell et al., 2014). Yet low signal-to-noise ratio leads to challenges in the monitoring and interpretation of passive ChlF (Liu et al., 2015).

SIF can be measured passively using unmanned aerial system (UAS), airborne or satellite instruments using narrow absorption lines in the solar irradiance spectrum (Fraunhofer lines) covering the 650–800 nm range, as well as using absorption lines in the Earth's atmosphere, such as the O_2 absorption lines (Mohammed et al., 2019; Porcar-Castell et al., 2014). Sub-nanometre scale spectral resolution spectrometers are classically used to retrieve SIF in the O_2-A and O_2-B absorption lines at 760.5 nm and 687.5 nm, respectively (referred to as SIF_{760} and SIF_{687}) (Frankenberg et al., 2018; Rascher et al., 2015). The SIF signal measured at the O_2-B line is very close to the chlorophyll absorption peak and is therefore very sensitive to reabsorption of ChlF by chlorophyll (Fig. 3).

The information in both O_2-bands is complementary, as they differ in three ways. First, SIF_{760} potentially carries information emitted by more of the canopy including lower leaf layers, while SIF_{687} only carries information from the upper canopy layers (Porcar-Castell et al., 2014). A second difference lies in the relative contribution of both photosystems to the retrieved SIF. While SIF_{760} originates from both PSI and PSII, SIF_{687} originates primarily from PSII (Drusch et al., 2017; Mohammed et al., 2019). Third, canopy scattering is more significant for SIF_{760} than SIF_{687} (Yang et al., 2019).

Even within these narrow absorption bands, the measured radiation does not uniquely contain information about SIF, but it is also affected by the surface reflectance and the atmospheric absorption and scattering. These factors can be corrected for by using fluorescence-free pixels (e.g., clouded ocean pixels). A first filtering approach is based on applying a single-vector decomposition (SVD), primarily for the solar absorption lines (Guanter et al., 2013; Joiner et al., 2013; Rossini et al.,

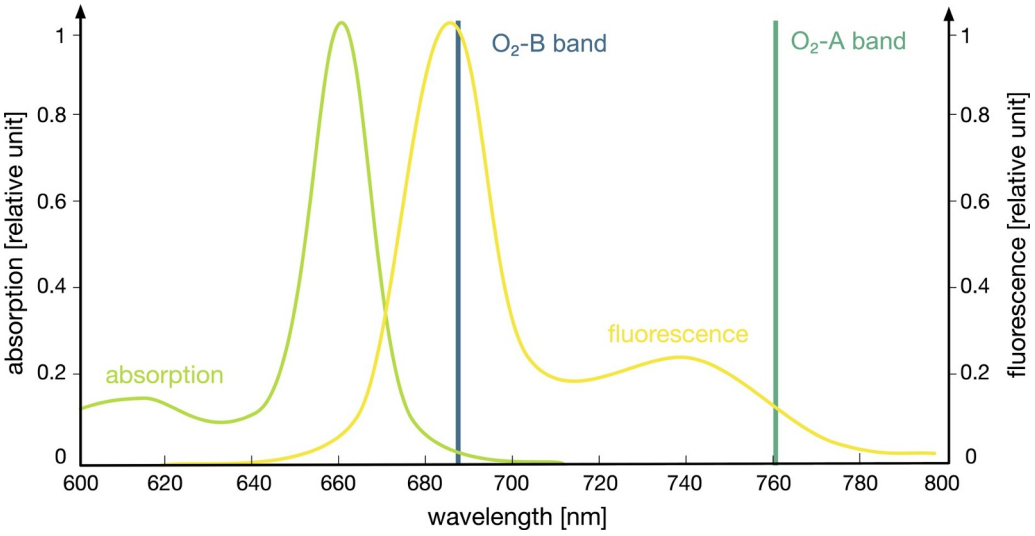

Fig. 3. Chlorophyll absorption and fluorescence spectra with oxygen absorption lines.

2015). SIF retrieved in these lines (e.g., TROPOMI SIF) is less affected by atmospheric absorption, therefore does not require substantial atmospheric modelling. The disadvantage of these lines is that they are neither deep nor wide. Consequently, a combination of several lines is required to retrieve a single SIF value (Köhler et al., 2018; Mohammed et al., 2019). A more sophisticated approach is the spectral filling method (SFM), which calculates the true reflectance, which is a smoothed line based on the reflectance in the wavelengths adjacent to the oxygen absorption lines. The difference between the measured reflectance and the simulated (true) reflectance provides an estimate of the SIF emission (Joiner et al., 2016). The upcoming FLEX mission will use an SFM-based approach (Cogliati et al., 2015), which will provide estimates of the entire fluorescence spectrum (Drusch et al., 2017). For a review of retrieval methods see Mohammed et al. (2019).

3.2. Global SIF observations

The first global space-based estimates of SIF became available in 2009 from TANSO-FTS aboard JAXA GOSAT, providing a coarse view of SIF emission at global scale (Frankenberg et al., 2011; Joiner et al., 2011). EUMETSAT´s Meteorological Operational satellites MetOp-A, -B and -C host the GOME-2 instrument, which is able to observe near-daily SIF at global scale (see an example of global map of GOME-2/MetOp-A SIF in Fig. 4). Joiner et al. (2013) proposed an alternative SIF retrieval method for GOME-2 by extending an SVD or principal component analysis technique applied exclusively on Fraunhofer lines (Guanter et al., 2012) to a broader wavelength range making also use of atmospheric absorption bands from water vapour and O_2-A. Importantly, Joiner et al. (2012) and Joiner et al. (2013) showed that instruments with lower spectral resolutions but better spatial coverage were also capable of retrieving SIF from space. This also applied to SCIAMACHY aboard EnviSat. It is worth noting that the GOME-2 instrument on MetOp-A (like GOME/ERS-2 and SCIAMACHY/EnviSat) is sensitive to continuous degradation attributed to prolonged exposure to solar radiation and contamination of optical elements. However the signal-to-noise ratio in the region around 740 nm is hardly affected and corrections have been proposed for the SIF retrievals (van Schaik et al., 2020).

The recently launched TROPOMI aboard Sentinel-5 Precursor allows almost daily observations at wide spectral sampling. This makes it possible to exploit the information of the full SIF spectrum and not only the longer wavelength peak in the near infrared. In recent years, radiative transfer models (RTMs) have been developed to simulate and interpret the SIF emission spectrum (van der Tol et al., 2009). Guanter et al. (2015) found from TROPOMI-like simulations with the FluorSAIL leaf and canopy RTM (Miller et al., 2003) that undetected clouds may be the largest error contribution during SIF retrieval; corrections are possible for properly identified clouds. Clouds cause a decrease in atmospheric transmittance across the spectral continuum. Recently, Köhler et al. (2018) presented the first TROPOMI-SIF retrievals, which match well with the higher spatial (but lower temporal) resolution OCO-2 retrievals (see an example of global TROPOMI and OCO-2 SIF in Fig. 4). A list of past, current and future satellite missions with the potential to estimate SIF is given in Table 2.

Up to now, global retrievals of SIF from space have only been achieved from spaceborne spectrometers designed to monitor atmospheric trace gases. These instrument are not optimal in terms of spectral sampling, overpass time and temporal resolution, and—most importantly—spatial resolution. Overpass time in particular may impact plant-water interactions as highlighted by the effect of increased afternoon water stress in more arid climates (Bonan et al., 2014; Guan et al., 2016).

The FLuorescence EXplorer (FLEX) is the first dedicated fluorescence mission by the European Space Agency (ESA). FLEX will become the 8th ESA Earth Explorer (Drusch et al., 2017) and is expected to launch in 2023. FLEX will fly in formation with the Sentinel-3 satellites ensuring simultaneous auxiliary measurements with a minimum impact of spatial and temporal co-location errors. This tandem schedule makes use of Sentinel-3′s atmospheric parameters (clouds, aerosols, water vapour) observations so that spectral fitting and Fraunhofer Line Depths-exploiting techniques can be implemented to decouple the fluorescence and reflectance signals from top-of-atmosphere measurements influenced by clouds and aerosols (Sabater et al., 2015). FLEX will host the Low Resolution Fluorescence Imaging Spectrometer (FLORIS LR), acquiring data in the red edge, chlorophyll absorption and Photochemical Reflectance Index bands (500–758 nm) with a spectral sampling width of 0.5–2.0 nm, and the High Resolution Fluorescence Imaging Spectrometer (FLORIS HR) with a sampling width of 0.1 nm in the two oxygen bands (677–697 nm and 740–780 nm) (Coppo et al., 2017). The tandem FLEX/Sentinel-3 mission will provide SIF data with significantly improved atmospheric corrections and SIF detection. FLEX/Sentinel-3 overpass time will be 10:00 at the Equator, meeting the optimal requirements to measure SIF from space (Drusch et al., 2017). However, FLEX will only allow a limited revisit frequency with a repeat cycle of 27 days, which is longer than the time scale of most hydrological processes.

Upcoming geostationary missions such as the Geostationary Carbon Cycle Observatory (GeoCarb), the Tropospheric Emissions: Monitoring of Pollution (TEMPO) and Sentinel-4 aboard the Meteosat Third Generation-Sounder (MTG-S) should have the capabilities for collecting multiple SIF observations a day over Europe and the Americas, but with lower spectral and spatial resolution compared to FLEX. Combining the complementary capabilities of FLEX and these geostationary missions should provide valuable information for monitoring plant water interactions.

3.3. Interpretation of spatially-aggregated SIF

At spatial scales coarser than a single leaf, plant or tree, SIF becomes an aggregated landscape variable, which depends on water in multiple ways (Joiner et al., 2014):

$$\mathrm{SIF}(\lambda) = \mathrm{PAR}\cdot \mathrm{fPAR}_{\mathrm{Chl}}\cdot \phi_{\mathrm{F}}(\lambda)\cdot \mathrm{f}_{\mathrm{esc}}(\lambda)\cdot \tau_{\mathrm{atm}}(\lambda) \quad (1)$$

The fraction of PAR absorbed by chlorophyll pigments, $\mathrm{fPAR}_{\mathrm{Chl}}$, is a function of vegetation cover fraction, LAI, leaf chlorophyll content, and plant structure—all of which depend on water availability and vary in time within a spatial pixel. The fluorescence quantum yield (ϕ_{F}), i.e., the ratio of the energy emitted by fluorescence and the absorbed radiation, is here taken as an averaged bulk property, which depends on the plant water status as described previously in Section 2. $\mathrm{f}_{\mathrm{esc}}$, i.e., the fraction of SIF emitted by the chloroplast that leaves the canopy, depends on LAI, leaf turgor, and the dynamic patterns of canopy structure. The fraction of SIF that leaves the top of canopy that also passes through the atmosphere (τ_{atm}) and the incident PAR are indirectly functions of water availability through cloud-, water vapour- and aerosol-driven atmospheric opacity and scattering, and can vary greatly from arid to humid conditions in time and space (Du et al., 2018; Köhler et al., 2018). All of these variables show both short-term variability (e.g., due to stress) as well as seasonal variability, providing SIF with a typical seasonal pattern, unique to each pixel (e.g., Lu et al., 2018). Fig. 5 shows the partitioning of radiation in plant canopies.

The effect of water on SIF across spatial scales is unclear, despite empirical work at the pixel scale (Alemohammad et al., 2017; Short Gianotti et al., 2019; Sun et al., 2015; Yoshida et al., 2015). Bulk relationships between typical land surface model variables (e.g., PAR, $\mathrm{fPAR}_{\mathrm{Chl}}$) and coarse water state variables (e.g., soil moisture, VPD) can perhaps be scaled from soil–plant–atmosphere continuum models. But the role of water status on ϕ_{F} is still an area of active research on physiological scales (see Table 2), and the timescales of ϕ_{F} fluctuations (on the order of seconds to minutes) (Flexas et al., 2000) are orders of magnitude different from those linking water to $\mathrm{fPAR}_{\mathrm{Chl}}$ via LAI (days to weeks) (Qiu et al., 2018). This leaves the SIF–water relations across

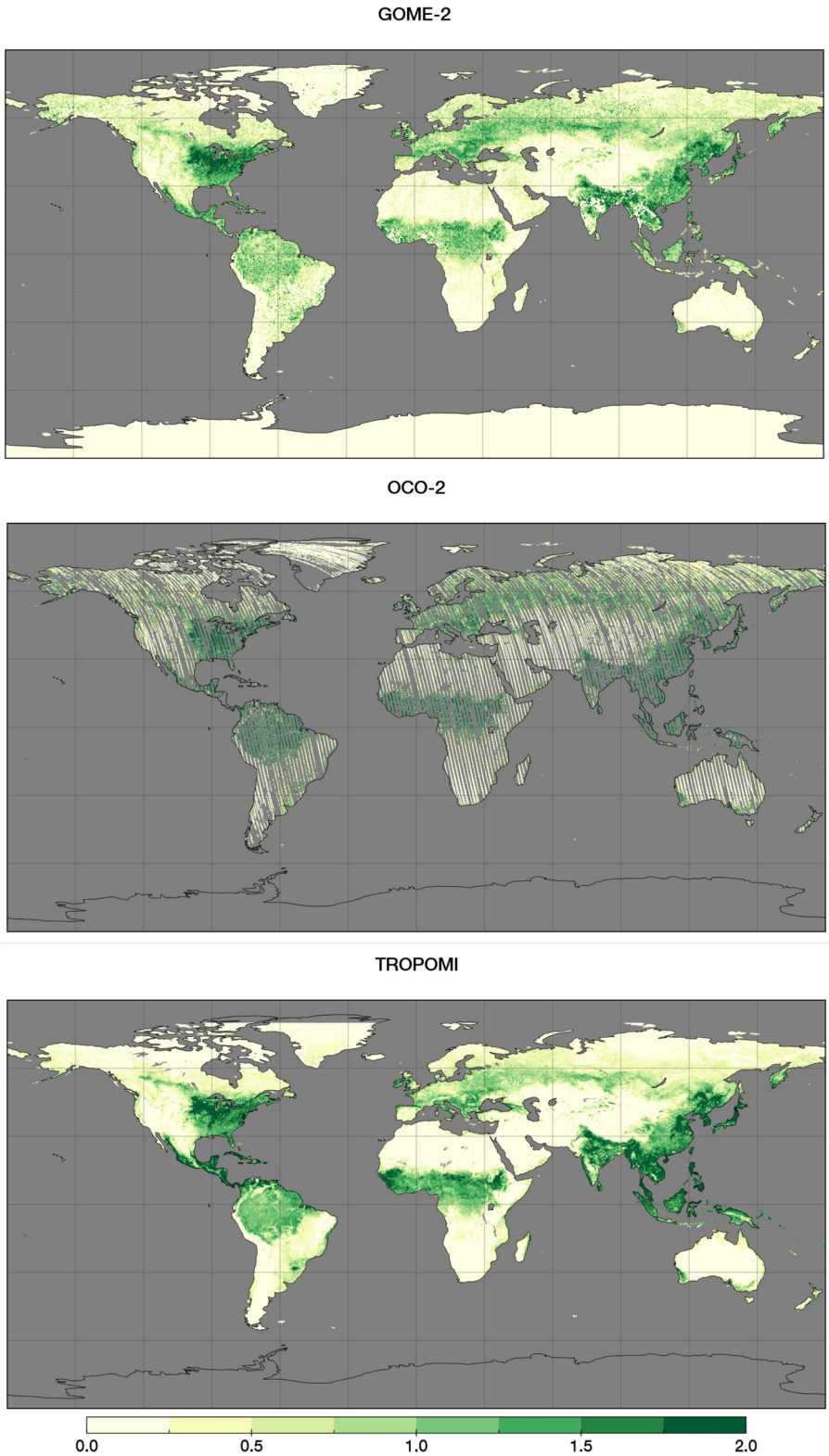

Fig. 4. Average global observations of sun-induced chlorophyll fluorescence (SIF) [mW m^{-2} nm^{-1} sr^{-1}] at 740 nm from GOME-2/MetOp-A (Köhler et al., 2015) (gridded to a spatial resolution of 0.5°), OCO-2 (Gunson and Eldering, 2017) (regridded to 0.25°) and TROPOMI/Sentinel-5P (Köhler et al., 2018) (regridded to 0.2°) for August 2018. OCO-2 SIF is scaled to 740 nm using the methodology from Köhler et al. (2018). Note that large gaps between orbit paths can be seen on the OCO-2 SIF map.

both space and time unconstrained.

Spatially-aggregated SIF is often taken as a proxy for spatially-aggregated GPP (e.g., Madani et al., 2017; Yang et al., 2018; Zhang et al., 2018b, 2016), based on correlations between GPP and right-hand terms of Eq. (1). As explained in Guanter et al. (2014) the most notable correlations come from $APAR_{Chl}$ ($= PAR \cdot fPAR_{Chl}$), which is seen in the light-use efficiency (LUE) model for GPP (Monteith, 1972; Monteith et al., 1977):

Table 2
Nominal mission design of past, current and future SIF-observing spaceborne sensors (adapted from Mohammed et al. (2019)). Despite the noted resolution, final SIF products typically require spatial and temporal averaging to reduce signal-to-noise ratio (ISS: International Space Station; ERS: European Remote Sensing; GEO: Geostationary Earth Orbit; CONUS: Contiguous United States).

Platform	Sensor	Observation period	Repeat cycle [day or hour]	Spatial resolution [km^2]	Overpass time [local time]	Spectral resolution [nm]	SIF spectral range [nm]
ERS-2	GOME	July 1995 – June 2003	3d	40 × 320	10:30	0.4	595–793
EnviSat	SCIAMACHY	Mar. 2002 – Apr. 2012	35d (3d for global mapping)	60 × 30	10:00	0.48	595–812
MetOp-A/B/C	GOME-2	Jan. 2007 – present (-A); Feb. 2013 – present (-B); Nov. 2018 – present (-C)	29d (1.5d for global mapping)	40 × 80 (MetOp-A until 2013); 40 × 40	9:30	0.5	593–790
GOSAT/GOSAT-2	TANSO-FTS/ TANSO-FTS-2	Jan. 2009 – present (GOSAT); Oct. 2019 – present (GOSAT-2)	3d (GOSAT); 6d (GOSAT-2) (3d for global mapping)	82 circular spatial footprint (10.5 km diameter)	13:00	0.025	758–775
OCO-2	OCO-2	Sept. 2014 – present	16d (16d for global mapping)	1.3 × 2.25	13:30	0.042	757–775
Sentinel-5P	TROPOMI	Oct. 2017 – present	16d (1d for global mapping)	7 × 7	13:30	0.5	675–775
TanSat	ACGS	Feb. 2018 – present	16d	2 × 3	13:30	0.044	758–778
ISS	OCO-3	May 2019 – present	variable	1.6 × 2.2	variable	0.05	757–775
TEMPO	TEMPO	2022	1h	4 × 5	GEO (CONUS)	0.6	540–740
GeoCarb	GeoCarb	2022	8h	~3 × 3	GEO (The Americas)	0.05	757–772
MTG-S	Sentinel-4	2022	1h	8 × 8	GEO (Europe)	0.12	750–775
FLEX	FLORIS LR/HR	2023	27d	0.3 × 0.3	10:00	0.5–2.0 (LR); 0.1 (HR)	500–780 (LR); 686–697 (HR); 759–769 (HR)

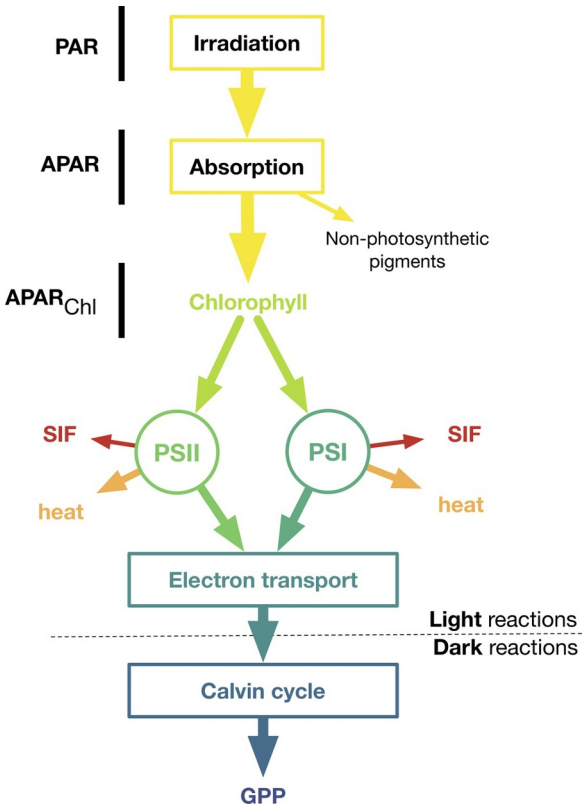

Fig. 5. Schematic representation of the radiation partitioning in plant canopies (modified from Porcar-Castell et al. (2014) and Zhang et al. (2018c)).

$$GPP \propto PAR \cdot fPAR_{Chl} \cdot \phi_P \quad (2)$$

with ϕ_P being the photochemical quantum yield. Combining Eqs. (1) and 2 (and setting aside the variability in f_{esc} and τ_{atm}), we see that the relationship between SIF and GPP is effectively scaled by the ratios of the fluorescence and photosynthetic quantum efficiencies ϕ_F/ϕ_P:

$$SIF \propto GPP \cdot \phi_F/\phi_P \quad (3)$$

Leaf-scale studies have shown that the ϕ_F - ϕ_P relationship is not always linear (Chen et al., 2018; van der Tol et al., 2014; Yang et al., 2018). We expect that this non-linearity at the photosystem level induced by heat or water stress might change the LUE or WUE, and thereby change the relationship between the canopy-scale variables of SIF and GPP. This relationship is classically considered linear at large temporal (days-months) and spatial (canopy-ecosystem) scales (Lee et al., 2015), potentially removing short-term non-linearities observed at leaf level. Dechant et al. (2020) identified canopy structure/absorption as the mechanistic tie between SIF and GPP (rather than ϕ_F) by showing that the product of APAR and f_{esc} predicted GPP better than SIF itself at diurnal to seasonal time scales and using canopy-level observations. Optically-based GPP estimates and SIF retrievals from GOME-2 both respond in the same fashion to soil moisture anomalies; dry anomalies lead to negative GPP and SIF anomalies in arid regions, with weaker responses in semi-arid regions, and no response in humid regions (Short Gianotti et al., 2019). This suggests that at remote sensing scales, the impacts of water stress may be more obvious in $APAR_{Chl}$ than in ϕ_F/ϕ_P energy partitioning.

The interpretation of remotely sensed SIF is hampered by confounding factors including canopy structure and light availability, affecting $APAR_{Chl}$ and biochemically controlled ϕ_F/ϕ_P (Yang et al., 2020, 2019). Quantifying the impacts of these confounding factors and their relationship with water availability is a necessary first step, however, in determining the role of water limitation on vegetation across spatial scales.

3.4. How remote sensing of SIF can contribute to transpiration monitoring?

Since the first release of GOSAT SIF data, satellite-based SIF retrievals have been mainly applied to estimate GPP, with a special emphasis on croplands (Frankenberg et al., 2011; Joiner et al., 2014; Madani et al., 2017; Sun et al., 2018). Since then, most studies have acknowledged the need for high-quality spaceborne SIF observations to study the terrestrial carbon cycles (see, e.g., Sun et al. (2017)). Process-based land surface models, especially those considering plant growth, require complex formulations to reliably estimate GPP (De Kauwe et al., 2015; Richardson et al., 2012). Remotely-sensed SIF data can be used to 1) directly parametrize sub-components of these models, 2) constrain model predictions of GPP, and 3) re-calibrate internal functions, such as the soil moisture stress functions (Lee et al., 2015; MacBean et al., 2018; Norton et al., 2018). Most land–surface models provide a flexible framework for data assimilation when executed offline, so that the simulation of the interplays between plant physiology and environmental factors can be constrained by SIF observations. More important to the context of this review, recent results support the potential of remotely sensed SIF to constrain not only GPP, but also transpiration fluxes in models (Alemohammad et al., 2017; Damm et al., 2018a; Green et al., 2017; Pagan et al., 2019; Rigden et al., 2018; Shan et al., 2019).

Despite being a crucial variable for global hydrology and climate, transpiration estimates remain largely uncertain at global scales, due to the scarcity of in situ measurements and the inability to retrieve transpiration directly from space (Damm et al., 2018a; Dolman et al., 2014; Li et al., 2019; McCabe et al., 2017). However, given the dependency of transpiration on stomatal conductance (g_s), and the expected relation of the latter to the SIF emission (Lu et al., 2018; Shan et al., 2019), current and future SIF retrievals represent a promising alternative to infer surface conductance and transpiration over large regions.

Alemohammad et al. (2017) presented the first framework (referred to as Water, Energy, and Carbon with Artificial Neural Networks or WECANN) to jointly retrieve transpiration and GPP using SIF observations at the global scale. Retrievals using SIF outperformed those using optical VIs in regions where water stress dominates seasonal variability, suggesting that SIF may detect changes in LUE not detected by optical VIs. Pagan et al. (2019) recently demonstrated the value of global SIF data to serve as a benchmark in climate model formulations of transpiration. By showing a high correlation of satellite-based SIF (normalised by PAR) to in situ estimates of transpiration efficiency derived from eddy-covariance measurements, their results suggested a high potential to improve offline land surface model simulations of water fluxes via SIF data assimilation. Rigden et al. (2018) found transpiration as a fraction of total evapotranspiration (ET) to be proportional to SIF divided by the local surface conductance. Moreover, Stoy et al. (2019) recently reviewed the current spectrum of techniques to partition transpiration and evaporation, and discussed the potential of SIF as a means to discriminate the transpiration component of ET.

The mechanistic links between SIF and transpiration are complex, and can perhaps be best examined in a coupled canopy radiation and land surface framework. The Soil Canopy Observation of Photochemistry and Energy fluxes (SCOPE) model (van der Tol et al., 2009) is an integrated radiative transfer and energy balance model and is well-suited for assimilation of SIF to constrain transpiration. SCOPE calculates the illumination of leaves with respect to their position and orientation in the canopy, and the spectra of reflected and emitted radiation above the canopy in the observation direction. Because it is a vertical one-dimensional model, running SCOPE at the global scale presents inherent challenges, especially related to its parametrization. However, the mechanistic representation of the biochemical processes related to SIF in SCOPE was incorporated in land surface models to constrain the photosynthesis estimates with SIF observations such as in the Community Land Model (CLM) 4 (Lee et al., 2015), in the Simplified Simple Biosphere Model 2.0 (SSiB2) (Qiu et al., 2018) or in the Biosphere Energy Transfer Hydrology (BETHY) land surface model (Norton et al., 2018). Damm et al. (2018b) presented the first canopy-scale study using SCOPE to assess the link between SIF and transpiration and its dependency on multiple meteorological and plant specific variables over multiple eddy-covariance sites, suggesting that SIF may be more sensitive to transpiration under water stress conditions. More recently, Maes et al. (private communication) applied the SCOPE model to the entire FLUXNET2015 database, and concluded that the relationship between SIF and transpiration is regulated by WUE. Despite the multiple environmental and biological factors determining WUE, it was concluded that accounting for the atmospheric demand for water, and in particular air temperature, helps explain most of the variability in the SIF–transpiration relationship at ecosystem scale. The line proposed by Maes et al. (private communication) to integrate observations (satellite, eddy covariance, and meteorological data) into RTMs appears a necessary step to increase understanding of the mechanistic relation between SIF and transpiration prior to using this relation to constrain hydrological and land surface models.

3.5. Remotely sensed SIF as an (early) drought diagnostic

Droughts cause agricultural loss, water scarcity, plant mortality (Choat et al., 2018) and air pollution (Demetillo et al., 2019), simultaneously increasing the occurrences of wild fires and endangering the sustainability of ecosystems and food production systems. As such, it is critical to forecast such events well in advance based on the water availability (through soil moisture and meteorology) and on the water demand (based on ET). As forecasting systems typically do not include any direct information concerning plant physiological functioning (see e.g., Otkin et al., 2018), these systems leave room for improvement concerning the detection of drought stress at the onset of drought (Sheffield et al., 2014; Weisheimer and Palmer, 2014). Accurate early warning is however imperative to allow the implementation of mitigation measures.

The three components of light energy partitioning (photosynthesis, heat dissipation, and chlorophyll fluorescence) behave differently when vegetation stress occurs. Negative anomalies in SIF, especially if normalized by $APAR_{Chl}$, are expected to integrate the effects of different environmental stressors on transpiration (Alemohammad et al., 2017; Cendrero-Mateo et al., 2015; Lu et al., 2018; Pagan et al., 2019). Disentangling the $APAR_{Chl}$ and ϕ_F components (see Eq. (1)) (Sun et al., 2015; Yang et al., 2019) as well as detecting the type of plant stress (drought, flooding, high/low temperature, wind, wildfire, nutrient availability, pesticides, plant disease, fungi, bacteria, insects, soil salinity, etc.) (Ač et al., 2015) is still an unresolved challenge for remotely-sensed SIF or simulations at larger scales (regional, continental). The $fPAR_{Chl}$ component—typically retrieved from the MODerate resolution Imaging Spectroradiometer (MODIS) aboard the National Aeronautics and Space Administration (NASA) Terra and Aqua satellites—is expected not to be sensitive to rapid changes in plant photosynthetic status (Song et al., 2018; Stocker et al., 2019). The ϕ_F component may be prone to faster changes during stress conditions (minutes to day) due to changes in the splitting of energy at PSII (van der Tol et al., 2014), hence it is the variable that holds the potential for early warning diagnosis.

The relationship between SIF and soil moisture plays out in three phases (Fig. 6). In the first phase, an increment in incoming radiation leads to an increment in SIF and in photosynthesis, until all chlorophyll/rubisco molecules are saturated (Tennessen et al., 1995; Wieneke et al., 2018). If the soil water content drops below a certain threshold (Phase II), the photosynthetic rate decreases due to stomatal and non-stomatal limitations (Section 2). The decrease in photosynthesis is linked to an increase in NPQ (Frankenberg and Berry, 2018). PAM-studies report an initial increase in ϕ_F caused by the decrease in photosynthesis, under mild stress conditions (Chen et al., 2018; van der Tol et al., 2014). However, in canopy-scale studies, stress results in a decrease in SIF_{760} (e.g., Wieneke et al., 2018; Wohlfahrt et al., 2018).

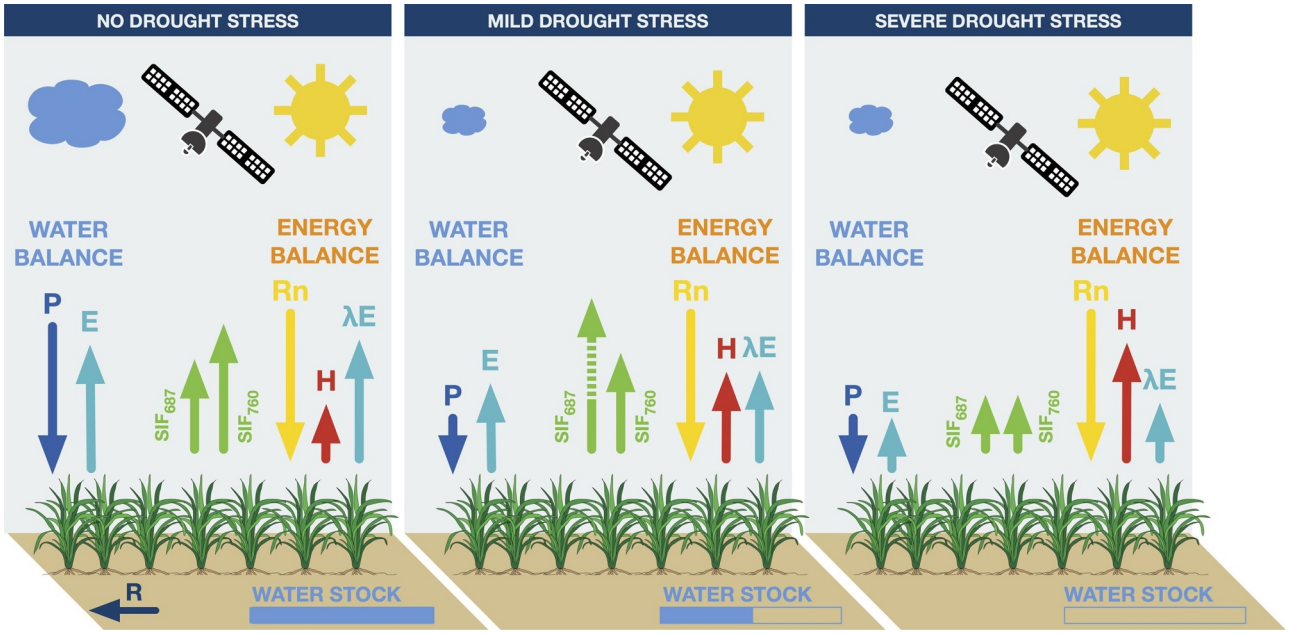

Fig. 6. Possible impact of soil water status on the water and energy balance and sun-induced chlorophyll fluorescence (SIF) at 687 nm and 760 nm (P: precipitation; E: evaporation; λE: latent heat flux; H: sensible heat flux; Rn: net radiation; R: runoff).

The behaviour of SIF_{687} is more ambiguous, since some canopy-scale studies suggest an increase in SIF_{687} at the timescale of a few days (Wohlfahrt et al., 2018) or an increase in SIF_{687}/SIF_{760} ratio (SIF_{ratio}) (Wieneke et al., 2016), while other studies suggest a decrease in SIF_{ratio} (Ač et al., 2015). The reaction of the canopy-scale SIF is the ensemble of the changes in the fluorescence emission at photosystem scale (van der Tol et al., 2014) and of changes in the canopy structure (Dechant et al., 2020; Yang et al., 2020, 2019). There are different possible explanations for the stress-induced change in SIF_{ratio}. A first explanation comes from the photosystem level. Since the relative contribution of both photosystems is different in both wavelengths (Mohammed et al., 2019), and since both photosystems react differently to stress (Agati et al., 2000), it is expected that a photosystem-driven change in the fluorescence emission modifies the shape of the fluorescence emission spectrum. A second explanation comes from structural changes, resulting in changes in different reabsorption and canopy scattering patterns (Yang et al., 2019). Looking beyond the timescale of a few days, the chlorophyll content decreases (Phase III), lowering both SIF_{687} and SIF_{760} (Buschmann, 2007; Sun et al., 2015; Wohlfahrt et al., 2018). As the partition of energy at photosystem level reacts very quickly to environmental stress, fluorescence may provide a means to detect vegetation drought stress in its earliest stage i.e., before chlorophyll reduction takes place.

Several studies at the global scale have shown that SIF is a good proxy for estimating ecosystem productivity, given its link to photosynthesis, outperforming classical optical vegetation indices (VIs) (Alemohammad et al., 2017; Koffi et al., 2015). This assessment is motivated by a generally slower response of greenness indices (which are more related to chlorophyll content and structural changes) to plant stress as compared to SIF yield, i.e., SIF normalized by APAR (which is directly affected by physiological regulation). The current state of the art spectrometers dedicated to the retrieval of SIF from an airborne platform are the imaging spectrometer HyPlant (Rascher et al., 2015; Siegmann et al., 2019) and the Chlorophyll Fluorescence Imaging Spectrometer (CFIS) (Frankenberg et al., 2018). Several studies with the HyPlant airborne sensor have contributed to a better understanding of the relationship between SIF and plant stress (Rossini et al., 2016; Wieneke et al., 2016). HyPlant campaigns over the Rur catchment area in Germany since 2015 have shown that SIF is linked to soil moisture and water availability in deeper soil layers (von Hebel et al., 2018), and combining airborne SIF and thermal observations has provided a framework on how to link several remote sensing approaches to map the complex functional properties of vegetation drought stress (Gerhards et al., 2018). It should be noted that airborne campaigns are logistically demanding and require clear-sky conditions, therefore only providing a few measurements a year over a limited area. Currently, prototypes of lightweight UAS-based spectrometers for SIF retrieval are being developed. These would allow providing SIF observations with an unprecedented spatial and temporal resolution (Gago et al., 2015). An early UAS-based study has shown that SIF could serve as a proxy for water potential and stomatal conductance at the local scale (Zarco-Tejada et al., 2012).

SIF observations from space may not directly reflect the drought impact on fluorescence quantum yield, but stress-induced changes in chlorophyll content and canopy structure, especially given the lower revisit time of current satellite observations. During a mild drought event a SIF reduction alone may occur, without concurrent changes in chlorophyll content and phenology (i.e., a decrease in ϕ_F, while APAR remains unchanged in Eq. (1)). In contrast, during extreme droughts, soil water deficit induces stomatal closure and hence a reduction of CO_2 uptake, which in turn slows down photosynthesis. Here, SIF reduction may be caused additionally by a reduction of APAR (Eq. (1)) that drives electron transport for carbon assimilation (Sun et al., 2015) or by higher VPD (Zhou et al., 2019). APAR can be reduced also by degraded photosynthetic pigments and a change in vegetation structure (by leaf wilting, plant turgor loss, leaf movement, leaf rolling) (Gentine et al., 2018). Yang et al. (2020) developed a method to isolate the plant physiological effects on the SIF signal from changes in chlorophyll content or plant structure. This could potentially lead to the detection of subtle, stress-induced changes in photosynthesis at large scale, enabling an early drought diagnostic. This detection can be enhanced by coincident observations of soil and vegetation moisture conditions, e.g., from the NASA Soil Moisture Active and Passive (SMAP) satellite (Fig. 7). Alternative stress conditions can easily be excluded in this way. Finally, it is also worth noting that the satellite overpass time is critical for using SIF to infer the vegetation photosynthesis response. Fluorescence yield can exhibit a diurnal variation related to diurnal changes of drought stress. Using SIF observation at different time of the day may

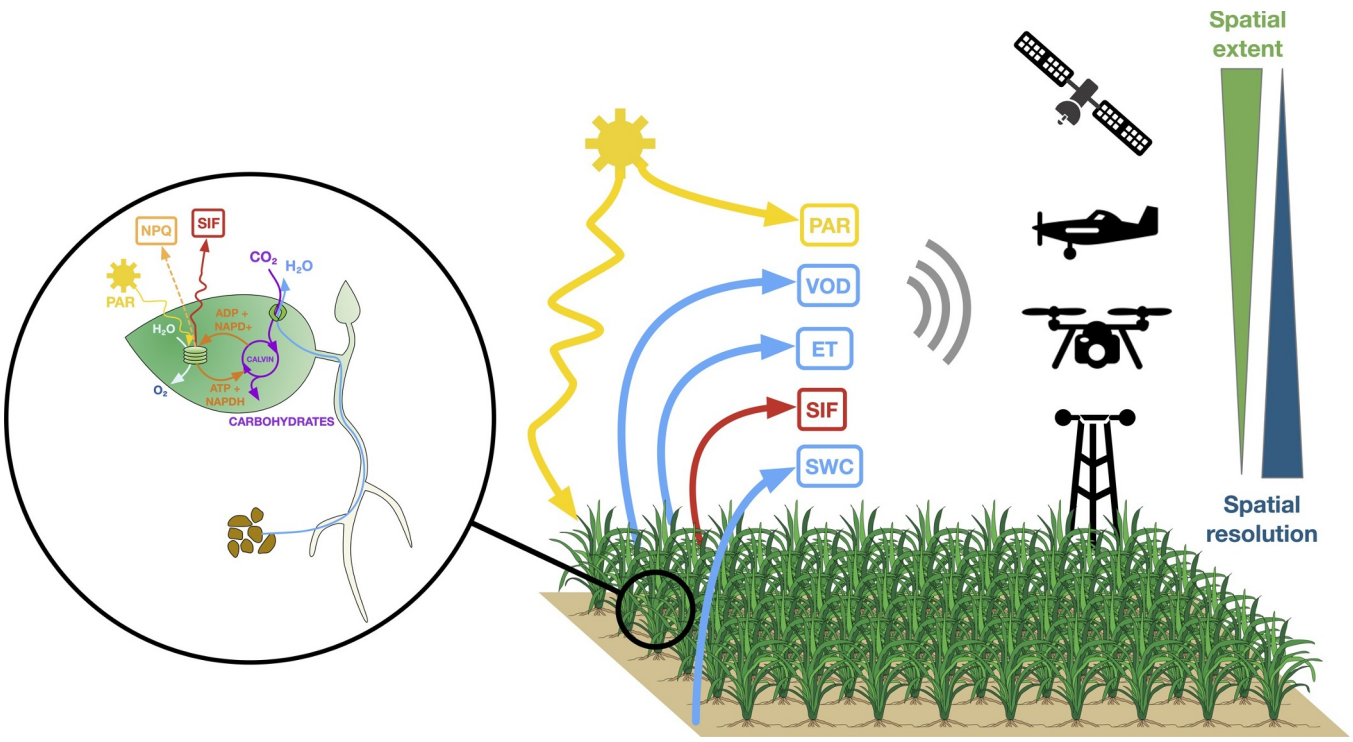

Fig. 7. Tower-based, UAS, and air-/space-borne remote sensing measurements of ecohydrologic variables (PAR: photosynthetically active radiation; VOD: vegetation optical depth; ET: evapotranspiration; SIF: sun-induced chlorophyll fluorescence; SWC: soil water content) from canopy to ecosystem scale.

therefore give different drought severity predictions (Zhang et al., 2018b).

4. Conclusion and challenges

In this paper we analyse the current status of using ChlF measurements to provide information on hydrological processes such as root water uptake, transpiration and the moisture status of the soil-root zone. Previous findings have shown the potential in using these measurements to constrain hydrological processes. In addition, new technologies have become available that are more accurate and allow upscaling from leaf to canopy and ecosystem scales. Several challenges need to be addressed to reach this goal. A first major challenge concerns the upscaling from leaf-scale fluorescence to canopy-scale SIF. At leaf-scale, the measurement signal can clearly be linked to the photosystem activity. Canopy-scale measurements are affected by reabsorption and canopy scattering, both depending on the chlorophyll content and the canopy structure. These factors have different effects on different wavelengths of the SIF emission spectrum. Relating canopy-scale SIF to leaf-scale PAM measurements will allow separating the contribution from the changes in physiological activity and changes in vegetation structure to changes in canopy-scale SIF emission.

The next challenge concerns upscaling canopy-scale SIF emission to the ecosystem scale. This is complicated both by spatial aggregation and temporal sampling. In the spatial domain, difficulties include the strong heterogeneity of the SIF emission due to spatial heterogeneity in environmental controls. Remotely sensed SIF retrievals necessarily confront the seasonal variations in each component of the SIF emission (Eq. (1)), biomass growth, and changing canopy characteristics. Here, UAS and airborne imagery (from, e.g., HyPlant or CFIS) play a crucial role, as they can measure the SIF emission at a metre-scale spatial resolution and a kilometre-scale spatial extent.

To model the effect of drought stress on SIF emission, RTMs must be adapted in a way that they can take drought stress into account. Therefore RTMs need to be coupled to plant and soil models to characterize the water status in both plant and soil compartments. In addition, field experiments, measuring both the water fluxes and canopy-scale SIF emission are needed to establish the link between soil moisture, drought stress and SIF emission. Once a clear link between SIF emission and drought stress has been established and incorporated in RTMs, SIF can provide information on the vegetation water status. This information can, in turn, be assimilated in land surface models and crop models, allowing these models to correct vegetation growth, carbon and water fluxes for drought stress.

The dependence of SIF emission on drought stress provides the opportunity for potential applications at canopy and ecosystem scales. At the canopy scale and for a constant APAR, the SIF signal would indicate stressed plants, enabling the optimization of precision irrigation systems. At the ecosystem scale, coupling SIF emission to a land surface model could lead to more precise GPP, LAI, and ET estimations, improving our understanding of the carbon and water cycle in the context of climate change.

Finally, there is a strong need to improve the retrieval of SIF—especially from satellites—and to quantify its uncertainty. Currently, the potential to improve land surface/hydrological modelling, especially for drought and transpiration monitoring, is hampered by the noise in the satellite SIF signal. Dedicated satellite missions such as FLEX are expected to provide less noisy SIF data. More frequent observations with a temporal resolution of less than one week are also required for typical hydrological applications. This will require a multi-sensor approach. To fully exploit the value of SIF, also the assimilation frameworks and the conceptual understanding need to be improved by the time these data streams will be available.

Declaration of competing interest

The authors declare that they have no known competing financial interests or personal relationships that could have appeared to influence the work reported in this paper.

Acknowledgments

This research was partially funded by the Deutsche Forschungsgemeinschaft (DFG, German Research Foundation) under Germany's Excellence Strategy - EXC 2070 – 390732324 and by the Fonds pour la Recherche dans l'Industrie et l'Agriculture (FRIA), Belgium. DGM and BRP acknowledge support from the European Research Council (ERC) under grant agreement 715254 (DRY–2–DRY) and the Belgian Science Policy Office (BELSPO) in the frame of the Support To Exploitation and Research in Earth Observation (STEREO) III programme project “Stress on TRanspiration Sensed from Satellite Sensors” (STR3S, SR/02/329). PG acknowledges NASA grant 80NSSC18K0998. FJ and DJSG acknowledge support from the Massachusetts Institute of Technology (MIT) with the MIT-Belgium Seed Fund “Early Detection of Plant Water Stress Using Remote Sensing”.

References

Ač, A, et al., 2015. Meta-analysis assessing potential of steady-state chlorophyll fluorescence for remote sensing detection of plant water, temperature and nitrogen stress. Remote Sens Environ 168, 420–436.
Acharya, B, Assmann, S., 2009. Hormone interactions in stomatal function. Plant Mol Biol 69 (4), 451–462.
Agati, G., Cerovic, Z.G, Moya, I., 2000. The Effect of Decreasing Temperature up to Chilling Values on the in vivo F685/F735 Chlorophyll Fluorescence Ratio in Phaseolus vulgaris and Pisum sativum: the Role of the Photosystem I Contribution to the 735 nm Fluorescence Band. Photochem. Photobiol. 72 (1), 75–84.
Alemohammad, S.H, et al., 2017. Water, Energy, and Carbon with Artificial Neural Networks (WECANN): a statistically based estimate of global surface turbulent fluxes and gross primary productivity using solar-induced fluorescence. Biogeosciences 14 (18), 4101–4124.
Barberon, M, et al., 2016. Adaptation of Root Function by Nutrient-Induced Plasticity of Endodermal Differentiation. Cell 164 (3), 447–459.
Bonan, G.B., Williams, M., Fisher, R.A, Oleson, K.W., 2014. Modeling stomatal conductance in the earth system: linking leaf water-use efficiency and water transport along the soil-plant-atmosphere continuum. Geosci Model Dev 7 (5), 2193–2222.
Bota, J., Tomas, M., Flexas, J., Medrano, H, Escalona, J.M., 2016. Differences among grapevine cultivars in their stomatal behavior and water use efficiency under progressive water stress. Agr Water Manage 164, 91–99.
Buschmann, C., 2007. Variability and application of the chlorophyll fluorescence emission ratio red/far-red of leaves. Photosynth Res 92 (2), 261–271.
Campos, H, et al., 2014. Photosynthetic acclimation to drought stress in Agave salmiana Otto ex Salm-Dyck seedlings is largely dependent on thermal dissipation and enhanced electron flux to photosystem I. Photosynth Res 122 (1), 23–39.
Carter, G.A., Jones, J.H., Mitchell, R.J, Brewer, C.H., 1996. Detection of solar-excited chlorophyll a fluorescence and leaf photosynthetic capacity using a fraunhofer line radiometer. Remote Sens Environ 55 (1), 89–92.
Cendrero-Mateo, M.P, et al., 2015. Dynamic response of plant chlorophyll fluorescence to light, water and nutrient availability. Funct Plant Biol 42 (8), 746–757.
Chen, X., Mo, X., Hu, S, Liu, S., 2018. Relationship between fluorescence yield and photochemical yield under water stress and intermediate light conditions. J Exp Bot 70 (1), 301–313.
Choat, B, et al., 2018. Triggers of tree mortality under drought. Nature 558 (7711), 531–539.
Christmann, A., Weiler, E.W., Steudle, E, Grill, E., 2007. A hydraulic signal in root-to-shoot signalling of water shortage. Plant J 52 (1), 167–174.
Cochard, H., 2002. Xylem embolism and drought-induced stomatal closure in maize. Planta 215 (3), 466–471.
Cochard, H., Barigah, S.T., Kleinhentz, M, Eshel, A., 2008. Is xylem cavitation resistance a relevant criterion for screening drought resistance among Prunus species? J Plant Physiol 165 (9), 976–982.
Cochard, H., Casella, E, Mencuccini, M., 2007a. Xylem vulnerability to cavitation varies among poplar and willow clones and correlates with yield. Tree Physiol 27 (12), 1761–1767.
Cochard, H, et al., 2007b. Putative role of aquaporins in variable hydraulic conductance of leaves in response to light. Plant Physiol 143 (1), 122–133.
Cogliati, S, et al., 2015. Retrieval of sun-induced fluorescence using advanced spectral fitting methods. Remote Sens Environ 169, 344–357.
Coppo, P, et al., 2017. Fluorescence Imaging Spectrometer (FLORIS) for ESA FLEX Mission. Remote Sens-Basel 9 (7).
Cousins, A.B, et al., 2002. Photosystem II energy use, non-photochemical quenching and the xanthophyll cycle in Sorghum bicolor grown under drought and free-air CO2 enrichment (FACE) conditions. Plant Cell Environ 25 (11), 1551–1559.
Damm, A, et al., 2018a. Remote sensing of plant-water relations: an overview and future perspectives. J Plant Physiol 227, 3–19.
Damm, A., Roethlin, S, Fritsche, L., 2018b. Towards Advanced Retrievals of Plant Transpiration Using Sun-Induced Chlorophyll Fluorescence: first Considerations. Int Geosci Remote Se 5983–5986.
De Kauwe, M.G, et al., 2015. Do land surface models need to include differential plant species responses to drought? Examining model predictions across a mesic-xeric gradient in Europe. Biogeosciences 12 (24), 7503–7518.
Dechant, B, et al., 2020. Canopy structure explains the relationship between photosynthesis and sun-induced chlorophyll fluorescence in crops. Remote Sens Environ 241, 111733.
Demetillo, M.A.G, et al., 2019. Observing Severe Drought Influences on Ozone Air Pollution in California. Environ Sci Technol 53 (9), 4695–4706.
Demmig-Adams, B., Cohu, C.M., Muller, O, Adams, W.W., 2012. Modulation of photosynthetic energy conversion efficiency in nature: from seconds to seasons. Photosynth Res 113 (1), 75–88.
Doblas, V.G, et al., 2017. Root diffusion barrier control by a vasculature-derived peptide binding to the SGN3 receptor. Science 355 (6322), 280–283.
Dolman, A.J., Miralles, D.G, de Jeu, R.A.M., 2014. Fifty years since Monteith's 1965 seminal paper: the emergence of global ecohydrology. Ecohydrology 7 (3), 897–902.
Drusch, M, et al., 2017. The FLuorescence EXplorer Mission Concept-ESA's Earth Explorer 8. Ieee T Geosci Remote 55 (3), 1273–1284.
Du, S, et al., 2018. Retrieval of global terrestrial solar-induced chlorophyll fluorescence from TanSat satellite. Science Bulletin 63 (22), 1502–1512.
Egea, G., Gonzalez-Real, M.M., Baille, A., Nortes, P.A., Diaz-Espejo, A., 2011. Disentangling the contributions of ontogeny and water stress to photosynthetic limitations in almond trees. Plant Cell Environ 34 (6), 962–979.
Enstone, D.E, Peterson, C.A., 2005. Suberin lamella development in maize seedling roots grown in aerated and stagnant conditions. Plant Cell Environ 28 (4), 444–455.
Feng, B, et al., 2014. Effect of Heat Stress on the Photosynthetic Characteristics in Flag Leaves at the Grain-Filling Stage of Different Heat-Resistant Winter Wheat Varieties. J Agron Crop Sci 200 (2), 143–155.
Flexas, J., Bota, J., Escalona, J.M., Sampol, B, Medrano, H., 2002a. Effects of drought on photosynthesis in grapevines under field conditions: an evaluation of stomatal and mesophyll limitations. Funct Plant Biol 29 (4), 461–471.
Flexas, J., Bota, J., Galmes, J., Medrano, H, Ribas-Carbo, M., 2006. Keeping a positive carbon balance under adverse conditions: responses of photosynthesis and respiration to water stress. Physiol Plantarum 127 (3), 343–352.
Flexas, J., Briantais, J.-.M., Cerovic, Z., Medrano, H, Moya, I., 2000. Steady-State and Maximum Chlorophyll Fluorescence Responses to Water Stress in Grapevine Leaves: a New Remote Sensing System. Remote Sens Environ 73 (3), 283–297.
Flexas, J, et al., 2016. Mesophyll conductance to CO2 and Rubisco as targets for improving intrinsic water use efficiency in C-3 plants. Plant Cell Environ 39 (5), 965–982.
Flexas, J, et al., 2002b. Steady-state chlorophyll fluorescence (Fs) measurements as a tool to follow variations of net CO2 assimilation and stomatal conductance during water-stress in C-3 plants. Physiol Plantarum 114 (2), 231–240.
Frankenberg, C, Berry, J., 2018. 3.10 - Solar Induced Chlorophyll Fluorescence: origins, Relation to Photosynthesis and Retrieval. Editor In: Liang, S (Ed.), Comprehensive Remote Sensing. Elsevier, Oxford, pp. 143–162.
Frankenberg, C, et al., 2011. New global observations of the terrestrial carbon cycle from GOSAT: patterns of plant fluorescence with gross primary productivity. Geophys Res Lett 38.
Frankenberg, C, et al., 2018. The Chlorophyll Fluorescence Imaging Spectrometer (CFIS), mapping far red fluorescence from aircraft. Remote Sens Environ 217, 523–536.
Frankenberg, C, et al., 2014. Prospects for chlorophyll fluorescence remote sensing from the Orbiting Carbon Observatory-2. Remote Sens Environ 147, 1–12.
Gago, J, et al., 2015. UAVs challenge to assess water stress for sustainable agriculture. Agr Water Manage 153, 9–19.
Gajanayake, B, Reddy, K.R., 2016. Sweetpotato Responses to Mid- and Late-Season Soil Moisture Deficits. Crop Sci 56 (4), 1865–1877.
Galmes, J., Medrano, H, Flexas, J., 2007. Photosynthetic limitations in response to water stress and recovery in Mediterranean plants with different growth forms. New Phytol 175 (1), 81–93.
Galmes, J., Molins, A., Flexas, J, Conesa, M.A., 2017. Coordination between leaf CO2 diffusion and Rubisco properties allows maximizing photosynthetic efficiency in Limonium species. Plant Cell Environ 40 (10), 2081–2094.
Gentine, P, Alemohammad, S.H., 2018. Reconstructed Solar-Induced Fluorescence: a Machine Learning Vegetation Product Based on MODIS Surface Reflectance to Reproduce GOME-2 Solar-Induced Fluorescence. Geophys Res Lett 45 (7), 3136–3146.
Gentine, P., Steeneveld, G.J., Heusinkveld, B.G, Holtslag, A.A.M., 2018. Coupling between radiative flux divergence and turbulence near the surface. Q J Roy Meteor Soc 144 (717), 2491–2507.
Gerhards, M, et al., 2018. Analysis of Airborne Optical and Thermal Imagery for Detection of Water Stress Symptoms. Remote Sens-Basel 10 (7), 1139.
Govindje, e, 1995. Sixty-Three Years Since Kautsky: chlorophyll *a* Fluorescence. Funct Plant Biol 22 (2), 131–160.
Grassi, G, Magnani, F., 2005. Stomatal, mesophyll conductance and biochemical limitations to photosynthesis as affected by drought and leaf ontogeny in ash and oak trees. Plant Cell Environ 28 (7), 834–849.
Green, J.K, et al., 2017. Regionally strong feedbacks between the atmosphere and terrestrial biosphere. Nat Geosci 10 (6), 410 -+.
Gu, L., Wood, J.D., Chang, C.Y.Y., Sun, Y, Riggs, J.S., 2019. Advancing Terrestrial Ecosystem Science With a Novel Automated Measurement System for Sun-Induced Chlorophyll Fluorescence for Integration With Eddy Covariance Flux Networks. J Geophys Res-Biogeo 124 (1), 127–146.
Guan, K.Y, et al., 2016. Improving the monitoring of crop productivity using spaceborne solar-induced fluorescence. Global Change Biol 22 (2), 716–726.
Guanter, L, et al., 2015. Potential of the TROPOspheric Monitoring Instrument (TROPOMI) onboard the Sentinel-5 Precursor for the monitoring of terrestrial chlorophyll fluorescence. Atmos Meas Tech 8 (3), 1337–1352.

Guanter, L, et al., 2012. Retrieval and global assessment of terrestrial chlorophyll fluorescence from GOSAT space measurements. Remote Sens Environ 121, 236–251.
Guanter, L, et al., 2013. Using field spectroscopy to assess the potential of statistical approaches for the retrieval of sun-induced chlorophyll fluorescence from ground and space. Remote Sens Environ 133, 52–61.
Guanter, L, et al., 2014. Global and time-resolved monitoring of crop photosynthesis with chlorophyll fluorescence. P Natl Acad Sci USA 111 (14), E1327–E1333.
Gunson, M, Eldering, A., 2017. In: DISC, G.E.S.D.a.I.S.C.G. (Ed.), Greenbelt, MD, USA (Editor).
Hachez, C, et al., 2012. Short-term control of maize cell and root water permeability through plasma membrane aquaporin isoforms. Plant Cell Environ 35 (1), 185–198.
Hose, E., Steudle, E, Hartung, W., 2000. Abscisic acid and hydraulic conductivity of maize roots: a study using cell- and root-pressure probes. Planta 211 (6), 874–882.
Huber, K, et al., 2014. Modelling the impact of heterogeneous rootzone water distribution on the regulation of transpiration by hormone transport and/or hydraulic pressures. Plant Soil 384 (1–2), 93–112.
IPCC, 2014. Contribution to the Fifth Assessment Report of the Intergovernmental Panel on Climate Change. Climate Change 2013: The Physical Science Basis. Cambridge UnivPress.
Jahns, P, Holzwarth, A.R., 2012. The role of the xanthophyll cycle and of lutein in photoprotection of photosystem II. Biochimica et Biophysica Acta (BBA) - Bioenergetics 1817 (1), 182–193.
Jarvis, P.G., 1976. Interpretation of Variations in Leaf Water Potential and Stomatal Conductance Found in Canopies in Field. Philos T Roy Soc B 273 (927), 593–610.
Jefferies, R.A., 1992. Effects of Drought on Chlorophyll Fluorescence in Potato (Solanum-Tuberosum L) .2. Relations between Plant-Growth and Measurements of Fluorescence. Potato Res 35 (1), 35–40.
Jin, E., Yokthongwattana, K., Polle, J.E.W, Melis, A., 2003. Role of the reversible xanthophyll cycle in the photosystem II damage and repair cycle in Dunaliella salina. Plant Physiol 132 (1), 352–364.
Joiner, J, et al., 2013. Global monitoring of terrestrial chlorophyll fluorescence from moderate-spectral-resolution near-infrared satellite measurements: methodology, simulations, and application to GOME-2. Atmos Meas Tech 6 (10), 2803–2823.
Joiner, J., Yoshida, Y., Guanter, L, Middleton, E.M., 2016. New methods for the retrieval of chlorophyll red fluorescence from hyperspectral satellite instruments: simulations and application to GOME-2 and SCIAMACHY. Atmos. Meas. Tech. 9 (8), 3939–3967.
Joiner, J, et al., 2014. The seasonal cycle of satellite chlorophyll fluorescence observations and its relationship to vegetation phenology and ecosystem atmosphere carbon exchange. Remote Sens Environ 152, 375–391.
Joiner, J, et al., 2012. Filling-in of near-infrared solar lines by terrestrial fluorescence and other geophysical effects: simulations and space-based observations from SCIAMACHY and GOSAT. Atmos Meas Tech 5 (4), 809–829.
Joiner, J, et al., 2011. First observations of global and seasonal terrestrial chlorophyll fluorescence from space. Biogeosciences 8 (3), 637–651.
Jonard, F., André, F., Ponette, Q., Vincke, C, Jonard, M., 2011. Sap flux density and stomatal conductance of European beech and common oak trees in pure and mixed stands during the summer drought of 2003. J Hydrol (Amst) 409, 371–381.
Kautsky, H, Hirsch, A., 1931. Neue Versuche zur Kohlensäureassimilation. Naturwissenschaften 19 (48), 964 -964.
Kebbas, S., Lutts, S, Aid, F., 2015. Effect of drought stress on the photosynthesis of Acacia tortilis subsp raddiana at the young seedling stage. Photosynthetica 53 (2), 288–298.
Keller, B, et al., 2019a. Genotype Specific Photosynthesis x Environment Interactions Captured by Automated Fluorescence Canopy Scans Over Two Fluctuating Growing Seasons. Front Plant Sci 10 (1482).
Keller, B, et al., 2019b. Maximum fluorescence and electron transport kinetics determined by light-induced fluorescence transients (LIFT) for photosynthesis phenotyping. Photosynth Res 140 (2), 221–233.
Kennedy, D, et al., 2019. Implementing Plant Hydraulics in the Community Land Model, Version 5. J Adv Model Earth Sy 11 (2), 485–513.
Koffi, E.N., Rayner, P.J., Norton, A.J., Frankenberg, C, Scholze, M., 2015. Investigating the usefulness of satellite-derived fluorescence data in inferring gross primary productivity within the carbon cycle data assimilation system. Biogeosciences 12 (13), 4067–4084.
Köhler, P, et al., 2018. Global Retrievals of Solar-Induced Chlorophyll Fluorescence With TROPOMI: first Results and Intersensor Comparison to OCO-2. Geophys Res Lett 45 (19), 10456–10463.
Köhler, P., Guanter, L, Joiner, J., 2015. A linear method for the retrieval of sun-induced chlorophyll fluorescence from GOME-2 and SCIAMACHY data. Atmos. Meas. Tech. 8 (6), 2589–2608.
Konings, A.G, Gentine, P., 2017. Global variations in ecosystem-scale isohydricity. Global Change Biol 23 (2), 891–905.
Konings, A.G., Piles, M., Das, N, Entekhabi, D., 2017. L-band vegetation optical depth and effective scattering albedo estimation from SMAP. Remote Sens Environ 198, 460–470.
Krause, G.H, Weis, E., 1991. Chlorophyll Fluorescence and Photosynthesis - the Basics. Annu Rev Plant Phys 42, 313–349.
Kruger, T.P.J, et al., 2012. Controlled Disorder in Plant Light-Harvesting Complex II Explains Its Photoprotective Role. Biophys J 102 (11), 2669–2676.
Lang, Y., Wang, M., Xia, J.B, Zhao, Q.K., 2018. Effects of soil drought stress on photosynthetic gas exchange traits and chlorophyll fluorescence in Forsythia suspensa. J Forestry Res 29 (1), 45–53.
Latrach, L, et al., 2014. Growth and nodulation of alfalfa-rhizobia symbiosis under salinity: electrolyte leakage, stomatal conductance, and chlorophyll fluorescence. Turk J Agric For 38 (3), 320–326.
Lee, J.E, et al., 2015. Simulations of chlorophyll fluorescence incorporated into the Community Land Model version 4. Global Change Biol 21 (9), 3469–3477.
Lemordant, L, Gentine, P., 2019. Vegetation Response to Rising CO2 Impacts Extreme Temperatures. Geophys Res Lett 46 (3), 1383–1392.
Lemordant, L., Gentine, P., Stefanon, M., Drobinski, P, Fatichi, S., 2016. Modification of land-atmosphere interactions by CO2 effects: implications for summer dryness and heat wave amplitude. Geophys Res Lett 43 (19), 10240–10248.
Li, S.W., Pezeshki, S.R, Goodwin, S., 2004. Effects of soil moisture regimes on photosynthesis and growth in cattail (Typha latifolia). Acta Oecol 25 (1–2), 17–22.
Li, X, et al., 2019. A simple and objective method to partition evapotranspiration into transpiration and evaporation at eddy-covariance sites. Agr Forest Meteorol 265, 171–182.
Lin, K.H., Hwang, W.C, Lo, H.F., 2007. Chilling stress and chilling tolerance of sweet potato as sensed by chlorophyll fluorescence. Photosynthetica 45 (4), 628–632.
Liu, L., Liu, X, Hu, J., 2015. Effects of spectral resolution and SNR on the vegetation solar-induced fluorescence retrieval using FLD-based methods at canopy level. European Journal of Remote Sensing 48 (1), 743–762.
Long, S.P, Bernacchi, C.J., 2003. Gas exchange measurements, what can they tell us about the underlying limitations to photosynthesis? Procedures and sources of error. J Exp Bot 54 (392), 2393–2401.
Lu, X.L, et al., 2018. Potential of solar-induced chlorophyll fluorescence to estimate transpiration in a temperate forest. Agr Forest Meteorol 252, 75.
MacBean, N, et al., 2018. Strong constraint on modelled global carbon uptake using solar-induced chlorophyll fluorescence data. Sci Rep-Uk 8.
Madani, N., Kimball, J.S., Jones, L.A., Parazoo, N.C, Guan, K.Y., 2017. Global Analysis of Bioclimatic Controls on Ecosystem Productivity Using Satellite Observations of Solar-Induced Chlorophyll Fluorescence. Remote Sens-Basel 9 (6).
Maes, W.H. et al., private communication. Ecosystem transpiration closely linked to sun-induced fluorescence as evidenced by satellite data and radiative transfer models.
Malenovský, Z., Mishra, K.B., Zemek, F., Rascher, U, Nedbal, L., 2009. Scientific and technical challenges in remote sensing of plant canopy reflectance and fluorescence. J Exp Bot 60 (11), 2987–3004.
Man, J.G., Yu, Z.W, Shi, Y., 2017. Radiation Interception, Chlorophyll Fluorescence and Senescence of Flag leaves in Winter Wheat under Supplemental Irrigation. Sci Rep-Uk 7.
Martin-StPaul, N., Delzon, S, Cochard, H., 2017. Plant resistance to drought depends on timely stomatal closure. Ecol Lett 20 (11), 1437–1447.
Martinez-Ballesta, M.C., Aparicio, F., Pallas, V., Martinez, V, Carvajal, M., 2003. Influence of saline stress on root hydraulic conductance and PIP expression in Arabidopsis. J Plant Physiol 160 (6), 689–697.
McCabe, M.F, et al., 2017. The future of Earth observation in hydrology. Hydrol Earth Syst Sc 21 (7), 3879–3914.
Medrano, H., Escalona, J.M., Bota, J., Gulias, J, Flexas, J., 2002. Regulation of photosynthesis of C-3 plants in response to progressive drought: stomatal conductance as a reference parameter. Ann Bot-London 89, 895–905.
Meroni, M, et al., 2009. Remote sensing of solar-induced chlorophyll fluorescence: review of methods and applications. Remote Sens Environ 113 (10), 2037–2051.
Miller, J.R, et al., 2003. Progress on the development of an integrated canopy fluorescence model. Igarss 2003: ieee International Geoscience and Remote Sensing Symposium. Vols I - Vii, Proceedings 601–603.
Mishra, K.B, et al., 2016. Chlorophyll a fluorescence, under half of the adaptive growth-irradiance, for high-throughput sensing of leaf-water deficit in Arabidopsis thaliana accessions. Plant Methods 12 (1), 46.
Mohammed, G.H, et al., 2019. Remote sensing of solar-induced chlorophyll fluorescence (SIF) in vegetation: 50 years of progress. Remote Sens Environ 231.
Momen, M, et al., 2017. Interacting Effects of Leaf Water Potential and Biomass on Vegetation Optical Depth. Journal of Geophysical Research. Biogeosciences: Medium: ED; Size 3031–3046.
Monteith, J.L., 1972. Solar Radiation and Productivity in Tropical Ecosystems. Journal of Applied Ecology 9 (3), 747–766.
Monteith, J.L., Moss, C.J., Cooke, G.W., Pirie, N.W, Bell, G.D.H., 1977. Climate and the efficiency of crop production in Britain. Philosophical Transactions of the Royal Society of London. B. Prog Nucl Energy 6 Biol Sci 281 (980), 277–294.
Moya, I, et al., 2004. A new instrument for passive remote sensing: 1. Measurements of sunlight-induced chlorophyll fluorescence. Remote Sens Environ 91 (2), 186–197.
Mulla, D.J., 2013. Twenty five years of remote sensing in precision agriculture: key advances and remaining knowledge gaps. Biosystems Engineering 114 (4), 358–371.
Murata, N., Allakhverdiev, S.I, Nishiyama, Y., 2012. The mechanism of photoinhibition in vivo: *re*-evaluation of the roles of catalase, α-tocopherol, non-photochemical quenching, and electron transport. Biochimica et Biophysica Acta (BBA) - Bioenergetics 1817 (8), 1127–1133.
Niyogi, K.K, Truong, T.B., 2013. Evolution of flexible non-photochemical quenching mechanisms that regulate light harvesting in oxygenic photosynthesis. Curr. Opin. Plant Biol. 16 (3), 307–314.
Norton, A.J., Rayner, P.J., Koffi, E.N, Scholze, M., 2018. Assimilating solar-induced chlorophyll fluorescence into the terrestrial biosphere model BETHY-SCOPE v1.0: model description and information content. Geosci Model Dev 11 (4), 1517–1536.
Novick, K.A., Konings, A.G, Gentine, P., 2019. Beyond soil water potential: an expanded view on isohydricity including land-atmosphere interactions and phenology. Plant Cell Environ 42 (6), 1802–1815.
Ohashi, Y., Nakayama, N., Saneoka, H, Fujita, K., 2006. Effects of drought stress on photosynthetic gas exchange, chlorophyll fluorescence and stem diameter of soybean plants. Biol Plantarum 50 (1), 138–141.
Omasa, K, Takayama, K., 2003. Simultaneous measurement of stomatal conductance, non-photochemical quenching, and photochemical yield of photosystem II in intact leaves by thermal and chlorophyll fluorescence imaging. Plant Cell Physiol 44 (12), 1290–1300.
Otkin, J.A., Zhong, Y.F., Lorenz, D., Anderson, M.C, Hain, C., 2018. Exploring seasonal

and regional relationships between the Evaporative Stress Index and surface weather and soil moisture anomalies across the United States. Hydrol Earth Syst Sc 22 (10), 5373–5386.
Pagan, B.R., Maes, W.H., Gentine, P., Martens, B, Miralles, D.G., 2019. Exploring the Potential of Satellite Solar-Induced Fluorescence to Constrain Global Transpiration Estimates. Remote Sens-Basel 11 (4).
Pettigrew, W.T., 2004. Physiological consequences of moisture deficit stress in cotton. Crop Sci 44 (4), 1265–1272.
Plascyk, J.A., 1975. Mk Ii Fraunhofer Line Discriminator (Fld-Ii) for Airborne and Orbital Remote-Sensing of Solar-Stimulated Luminescence. Opt Eng 14 (4), 339–346.
Porcar-Castell, A, et al., 2014. Linking chlorophyll a fluorescence to photosynthesis for remote sensing applications: mechanisms and challenges. J Exp Bot 65 (15), 4065–4095.
Qiu, B, et al., 2018. Satellite Chlorophyll Fluorescence and Soil Moisture Observations Lead to Advances in the Predictive Understanding of Global Terrestrial Coupled Carbon-Water Cycles. Global Biogeochem Cy 32 (3), 360–375.
Rascher, U, et al., 2015. Sun-induced fluorescence - a new probe of photosynthesis: first maps from the imaging spectrometer HyPlant. Global Change Biol 21 (12), 4673–4684.
Reed, D.W., 1969. Isolation and Composition of a Photosynthetic Reaction Center Complex from Rhodopseudomonas Spheroides. J Biol Chem 244 (18), 4936 -&.
Rewald, B., Ephrath, J.E, Rachmilevitch, S., 2011. A root is a root is a root? Water uptake rates of Citrus root orders. Plant Cell Environ 34 (1), 33–42.
Richardson, A.D, et al., 2012. Terrestrial biosphere models need better representation of vegetation phenology: results from the North American Carbon Program Site Synthesis. Global Change Biol 18 (2), 566–584.
Rigden, A.J., Salvucci, G.D., Entekhabi, D, Gianotti, D.J.S., 2018. Partitioning Evapotranspiration Over the Continental United States Using Weather Station Data. Geophys Res Lett 45 (18), 9605–9613.
Rochaix, J.D., 2007. Role of thylakoid protein kinases in photosynthetic acclimation. Febs Lett 581 (15), 2768–2775.
Rossini, M, et al., 2016. Analysis of Red and Far-Red Sun-Induced Chlorophyll Fluorescence and Their Ratio in Different Canopies Based on Observed and Modeled Data. Remote Sens-Basel 8 (5), 412.
Rossini, M, et al., 2015. Red and far red Sun-induced chlorophyll fluorescence as a measure of plant photosynthesis. Geophys Res Lett 42 (6), 1632–1639.
Ruban, A.V., 2016. Nonphotochemical Chlorophyll Fluorescence Quenching: mechanism and Effectiveness in Protecting Plants from Photodamage. Plant Physiol 170 (4), 1903–1916.
Sabater, N, et al., 2015. A Sun-Induced Vegetation Fluorescence Retrieval Method from Top of Atmosphere Radiance for the Flex/Sentinel-3 Tandem Mission. 2015. In: Ieee International Geoscience and Remote Sensing Symposium (Igarss), pp. 2669–2672.
Sade, N., Gebremedhin, A, Moshelion, M., 2012. Risk-taking plants: anisohydric behavior as a stress-resistance trait. Plant Signal Behav 7 (7), 767–770.
Sade, N, et al., 2009. Improving plant stress tolerance and yield production: is the tonoplast aquaporin SlTIP2;2 a key to isohydric to anisohydric conversion? New Phytol 181 (3), 651–661.
Schreiber, U., Schliwa, U, Bilger, W., 1986. Continuous Recording of Photochemical and Nonphotochemical Chlorophyll Fluorescence Quenching with a New Type of Modulation Fluorometer. Photosynth Res 10 (1–2), 51–62.
Shan, N, et al., 2019. Modeling canopy conductance and transpiration from solar-induced chlorophyll fluorescence. Agr Forest Meteorol 268, 189–201.
Sheffield, J, et al., 2014. A Drought Monitoring and Forecasting System for Sub-Sahara African Water Resources and Food Security. B Am Meteorol Soc 95 (6), 861 -+.
Short Gianotti, D.J., Rigden, A.J., Salvucci, G.D, Entekhabi, D., 2019. Satellite and Station Observations Demonstrate Water Availability's Effect on Continental-Scale Evaporative and Photosynthetic Land Surface Dynamics. Water Resour. Res. 55 (1), 540–554.
Siegmann, B, et al., 2019. The High-Performance Airborne Imaging Spectrometer HyPlant—From Raw Images to Top-of-Canopy Reflectance and Fluorescence Products: introduction of an Automatized Processing Chain. Remote Sens-Basel 11 (23), 2760.
Siqueira, M., Katul, G, Porporato, A., 2009. Soil Moisture Feedbacks on Convection Triggers: the Role of Soil-Plant Hydrodynamics. J Hydrometeorol 10 (1), 96–112.
Snider, J.L., Collins, G.D., Whitaker, J., Perry, C.D, Chastain, D.R., 2014. Electron Transport Through Photosystem II Is Not Limited By A Wide Range of Water Deficit Conditions In Field-Grown Gossypium hirsutum. J Agron Crop Sci 200 (1), 77–82.
Song, L, et al., 2018. Satellite sun-induced chlorophyll fluorescence detects early response of winter wheat to heat stress in the Indian Indo-Gangetic Plains. Global Change Biol 24 (9), 4023–4037.
Sperdouli, I, Moustakas, M., 2012. Interaction of proline, sugars, and anthocyanins during photosynthetic acclimation of Arabidopsis thaliana to drought stress. J Plant Physiol 169 (6), 577–585.
Sperry, J.S, et al., 2016. Pragmatic hydraulic theory predicts stomatal responses to climatic water deficits. New Phytol 212 (3), 577–589.
Stepien, P, Klobus, G., 2006. Water relations and photosynthesis in Cucumis sativus L. leaves under salt stress. Biol Plantarum 50 (4), 610–616.
Stirbet, A., Lazár, D., Kromdijk, J, Govindjee, 2018. Chlorophyll a fluorescence induction: can just a one-second measurement be used to quantify abiotic stress responses? Photosynthetica 56 (1), 86–104.
Stocker, B.D, et al., 2019. Drought impacts on terrestrial primary production underestimated by satellite monitoring. Nat Geosci 12 (4), 264–270.
Stoy, P.C, et al., 2019. Reviews and syntheses: turning the challenges of partitioning ecosystem evaporation and transpiration into opportunities. Biogeosciences 16 (19), 3747–3775.
Sun, Y, et al., 2018. Overview of Solar-Induced chlorophyll Fluorescence (SIF) from the Orbiting Carbon Observatory-2: retrieval, cross-mission comparison, and global monitoring for GPP. Remote Sens Environ 209, 808–823.
Sun, Y, et al., 2017. OCO-2 advances photosynthesis observation from space via solar-induced chlorophyll fluorescence. Science 358 (6360).
Sun, Y, et al., 2015. Drought onset mechanisms revealed by satellite solar-induced chlorophyll fluorescence: insights from two contrasting extreme events. J Geophys Res-Biogeo 120 (11), 2427–2440.
Tardieu, F., Simonneau, T, Parent, B., 2015. Modelling the coordination of the controls of stomatal aperture, transpiration, leaf growth, and abscisic acid: update and extension of the Tardieu-Davies model. J Exp Bot 66 (8), 2227–2237.
Tennessen, D.J., Bula, R.J, Sharkey, T.D., 1995. Efficiency of photosynthesis in continuous and pulsed light emitting diode irradiation. Photosynth Res 44 (3), 261–269.
Theisen, A.F., 2002. Detecting Chlorophyll Fluorescence from Orbit: the Fraunhofer Line Depth Model. From Laboratory Spectroscopy to Remotely Sensed Spectra of Terrestrial Ecosystems. Springer, Netherlands, pp. 203–232.
Trigo-Cordoba, E., Bouzas-Cid, Y., Orriols-Fernandez, I, Miras-Avalos, J.M., 2015. Effects of deficit irrigation on the performance of grapevine (Vitis vinifera L.) cv. 'Godello' and 'Treixadura' in Ribeiro, NW Spain. Agr Water Manage 161, 20–30.
van der Tol, C., Berry, J.A., Campbell, P.K.E, Rascher, U., 2014. Models of fluorescence and photosynthesis for interpreting measurements of solar-induced chlorophyll fluorescence. J Geophys Res-Biogeo 119 (12), 2312–2327.
van der Tol, C., Verhoef, W., Timmermans, J., Verhoef, A, Su, Z., 2009. An integrated model of soil-canopy spectral radiances, photosynthesis, fluorescence, temperature and energy balance. Biogeosciences 6 (12), 3109–3129.
van Schaik, E, et al., 2020. Improved SIFTER v2 algorithm for long-term GOME-2A satellite retrievals of fluorescence with a correction for instrument degradation. Atmos. Meas. Tech. Discuss. 2020, 1–33.
Vanlerberghe, G.C., Martyn, G.D., Dahal, K., 2016. Alternative oxidase: a respiratory electron transport chain pathway essential for maintaining photosynthetic performance during drought stress. Physiol Plantarum 157 (3), 322–337.
Vereecken, H., Weihermuller, L., Jonard, F., Montzka, C., 2012. Characterization of Crop Canopies and Water Stress Related Phenomena using Microwave Remote Sensing Methods: a Review. Vadose Zone J 11 (2).
Vincent, C., Rowland, D.L., Schaffer, B., 2015. The potential for primed acclimation in papaya (Carica papaya L.): determination of critical water deficit thresholds and physiological response variables. Sci Hortic-Amsterdam 194, 344–352.
von Hebel, C., et al., 2018. Understanding Soil and Plant Interaction by Combining Ground-Based Quantitative Electromagnetic Induction and Airborne Hyperspectral Data. Geophys Res Lett 45 (15), 7571–7579.
Wang, X.B., Wang, L.F., Shangguan, Z., 2016. Leaf Gas Exchange and Fluorescence of Two Winter Wheat Varieties in Response to Drought Stress and Nitrogen Supply. PLoS ONE 11 (11).
Weisheimer, A., Palmer, T.N., 2014. On the reliability of seasonal climate forecasts. J R Soc Interface 11 (96).
Wieneke, S, et al., 2016. Airborne based spectroscopy of red and far-red sun-induced chlorophyll fluorescence: implications for improved estimates of gross primary productivity. Remote Sens Environ 184, 654–667.
Wieneke, S., et al., 2018. Linking photosynthesis and sun-induced fluorescence at sub-daily to seasonal scales. Remote Sens Environ 219, 247–258.
Wohlfahrt, G, et al., 2018. Sun-induced fluorescence and gross primary productivity during a heat wave. Sci Rep-Uk 8 (1), 14169.
Wu, F.Z., Bao, W.K., Li, F.L, Wu, N., 2008. Effects of water stress and nitrogen supply on leaf gas exchange and fluorescence parameters of Sophora davidii seedlings. Photosynthetica 46 (1), 40–48.
Xia, J.B., Zhang, G.C., Wang, R.R., Zhang, S.Y., 2014. Effect of soil water availability on photosynthesis in Ziziphus jujuba var. spinosus in a sand habitat formed from seashells: comparison of four models. Photosynthetica 52 (2), 253–261.
Xu, Q., et al., 2020. Effects of Water Stress on Fluorescence Parameters and Photosynthetic Characteristics of Drip Irrigation in Rice. Water (Basel) 12 (1), 289.
Xu, Z.Z., Zhou, G.S., 2011. Responses of photosynthetic capacity to soil moisture gradient in perennial rhizome grass and perennial bunchgrass. Bmc Plant Biol 11.
Yang, K., et al., 2018. Sun-induced chlorophyll fluorescence is more strongly related to absorbed light than to photosynthesis at half-hourly resolution in a rice paddy. Remote Sens Environ 216, 658–673.
Yang, P., van der Tol, C., Campbell, P.K.E., Middleton, E.M., 2020. Fluorescence Correction Vegetation Index (FCVI): a physically based reflectance index to separate physiological and non-physiological information in far-red sun-induced chlorophyll fluorescence. Remote Sens Environ 240, 111676.
Yang, P., et al., 2019. Using reflectance to explain vegetation biochemical and structural effects on sun-induced chlorophyll fluorescence. Remote Sens Environ 231, 110996.
Yoshida, Y., et al., 2015. The 2010 Russian drought impact on satellite measurements of solar-induced chlorophyll fluorescence: insights from modeling and comparisons with parameters derived from satellite reflectances. Remote Sens Environ 166, 163–177.
Zarco-Tejada, P.J., Gonzalez-Dugo, V., Berni, J.A.J., 2012. Fluorescence, temperature and narrow-band indices acquired from a UAV platform for water stress detection using a micro-hyperspectral imager and a thermal camera. Remote Sens Environ 117, 322–337.
Zhang, Y., Joiner, J., Alemohammad, S.H., Zhou, S., Gentine, P., 2018a. A global spatially contiguous solar-induced fluorescence (CSIF) dataset using neural networks. Biogeosciences 15 (19), 5779–5800.
Zhang, Y., Joiner, J., Gentine, P., Zhou, S., 2018b. Reduced solar-induced chlorophyll fluorescence from GOME-2 during Amazon drought caused by dataset artifacts. Global Change Biol 24 (6), 2229–2230.
Zhang, Y., et al., 2016. Precipitation and carbon-water coupling jointly control the interannual variability of global land gross primary production. Sci Rep-Uk 6.

Zhang, Y., et al., 2018c. Spatio-Temporal Convergence of Maximum Daily Light-Use Efficiency Based on Radiation Absorption by Canopy Chlorophyll. Geophys Res Lett 45 (8), 3508–3519.
Zhang, Y., Zhou, S., Gentine, P, Xiao, X., 2019. Can vegetation optical depth reflect changes in leaf water potential during soil moisture dry-down events? Remote Sens Environ 234.
Zhou, L, et al., 2015. Responses of photosynthetic parameters to drought in subtropical forest ecosystem of China. Sci Rep-Uk 5.
Zhou, S., Zhang, Y., Williams, A.P., Gentine, P., 2019. Projected increases in intensity, frequency, and terrestrial carbon costs of compound drought and aridity events. Sci Adv 5 (1).
Zhou, S.X., Duursma, R.A., Medlyn, B.E., Kelly, J.W.G., Prentice, I.C., 2013. How should we model plant responses to drought? An analysis of stomatal and non-stomatal responses to water stress. Agr Forest Meteorol 182, 204–214.
Zivcak, M., et al., 2013. Photosynthetic electron transport and specific photoprotective responses in wheat leaves under drought stress. Photosynth Res 117 (1–3), 529–546.
Zwieniecki, M.A., Holbrook, N.M., 2009. Confronting Maxwell's demon: biophysics of xylem embolism repair. Trends Plant Sci 14 (10), 530–534.